Measurements of the inclusive isolated-photon and photon-plus-jet production in pp collisions at $\sqrt{s} = 13$ TeV with the ATLAS detector

Daniel Camarero, Brandeis University

IFIC Topical Seminar, Valencia, 18 November 2022

Outline

- **Prompt-photon production at the LHC**
  - Motivation
- **Photons and jets with the ATLAS detector**
  - Reconstruction, identification, calibration and isolation of photons and background subtraction in ATLAS
  - Jet reconstruction and calibration in ATLAS
- **Perturbative QCD theoretical calculations**
- **Inclusive-photon production and its dependence on photon isolation in pp collisions at $\sqrt{s} = 13$ TeV using 139 fb^{-1} of ATLAS data**
- **Measurement of the isolated photon plus jet cross section in pp collisions at $\sqrt{s} = 13$ TeV using the full Run-2 ATLAS data**
- **Summary and conclusions**

Prompt-photon production at the LHC

Prompt photon production at the LHC

The production of high-p_{T} prompt photons proceeds via two mechanisms:
(**prompt photon:** photon not coming from hadron decays.)

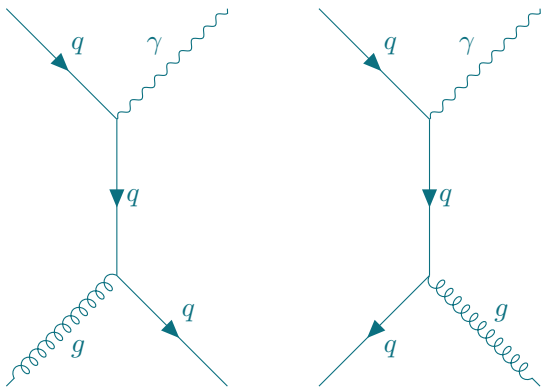

DIRECT

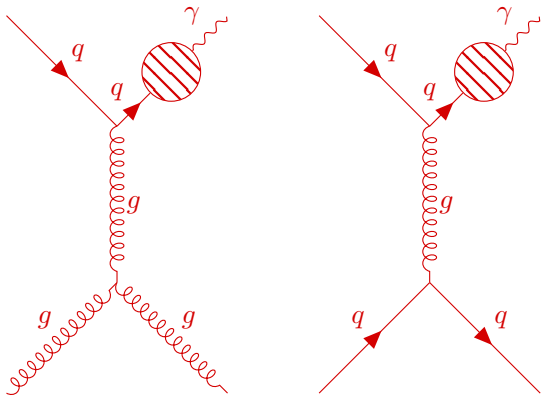

FRAGMENTATION

Measurements of prompt-photon production inclusively and in association with jets allow tests of pQCD at large Q^2 and over a wide range of x,

- provide experimental information to constrain the proton PDFs;
  (sensitivity to the gluon PDF already at LO via $qg \to q\gamma$)
- are useful to develop pQCD calculations and tune MC models;
- provide data to constrain the photon fragmentation functions.
- Photon+jet events are also useful to derive jet energy scale and resolution calibrations.

Prompt photon production at the LHC

Fragmentation prompt-photons:

The cross section contains a piece of the form $\hat{\sigma}^{\mathrm{dijet}} \otimes D^{\gamma}_{q/g}\left(z, \mu_{\mathrm{f}}^2\right)$, and is effectively of $\mathcal{O}\left(\alpha_{\mathrm{EM}}\alpha_{\mathrm{S}}\right)$ (same as direct).

Photons from hadron decays:

Photons are copiously produced inside jets due to neutral meson decays such as π^0 and η.

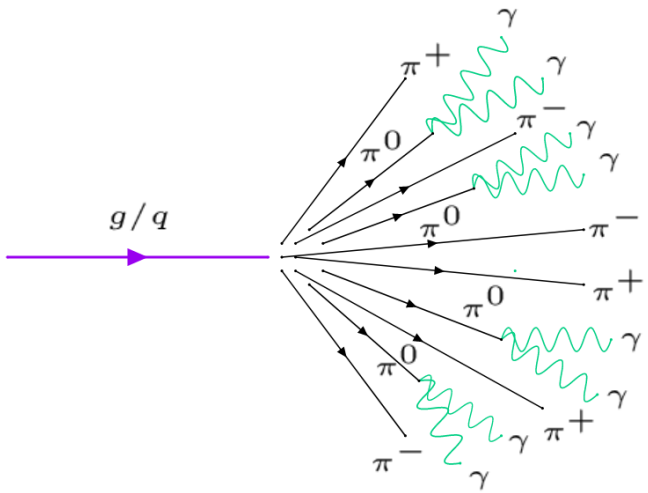

→ **Isolation requirement:** mostly suppresses the contribution of photons inside jets and the fragmentation-photon processes.

Before isolation requirement

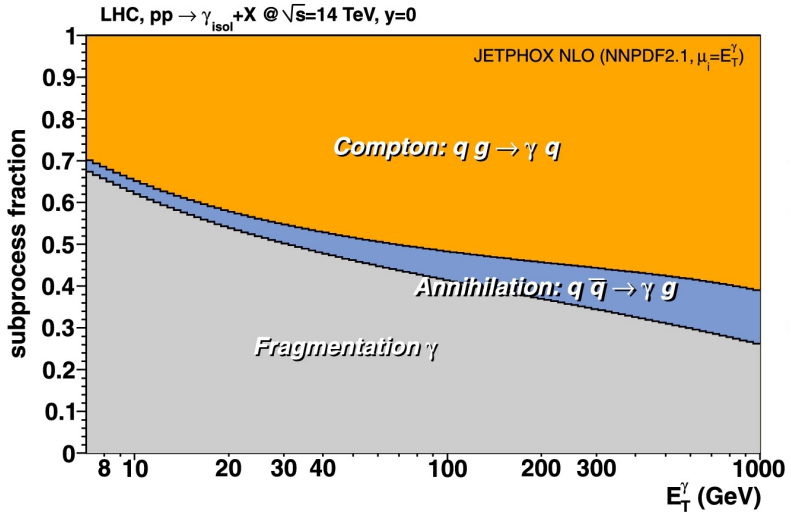

After isolation requirement

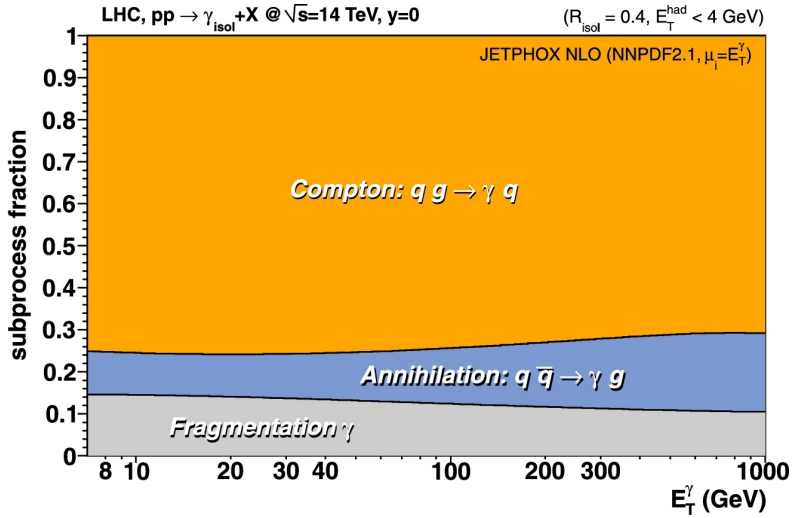

D. d'Enterria and J. Rojo, Nucl. Phys. B **860** (2012) 311

Prompt photon production at the LHC: isolation

Fixed-cone isolation: used at experimental level, requires the isolation transverse energy ($E_{\mathrm{T}}^{\mathrm{iso}}$) to fulfil

$$E_{\mathrm{T}}^{\mathrm{iso}} \equiv \sum_{\mathrm{i}} E_{\mathrm{T}}^{\mathrm{i}} < E_{\mathrm{T}}^{\mathrm{max}},$$

summing over the particles (except the photon) inside a cone of radius $\mathcal{R}$ centred on the photon in the $\eta - \phi$ plane.

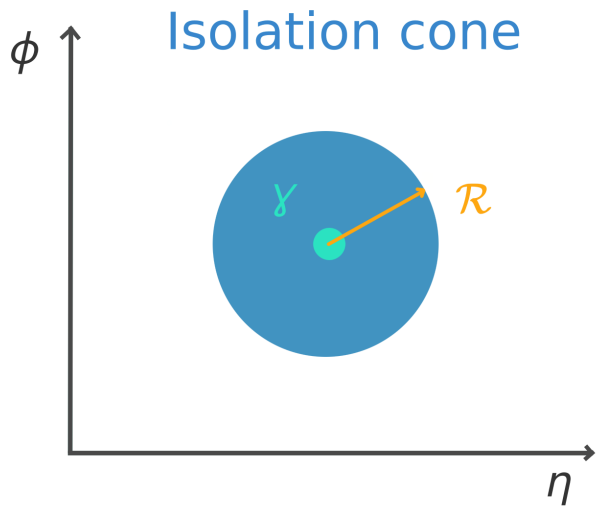

Smooth-cone (Frixione's) isolation: used in theoretical predictions, simplifies considerably the calculations by requiring

$$E_{\mathrm{T}}^{\mathrm{max}}(\mathcal{V}) = \epsilon\, E_{\mathrm{T}}^{\gamma} \left(\frac{1-\cos(\mathcal{V})}{1-\cos(\mathcal{R})} \right)^{n}, \forall\ \mathcal{V} < \mathcal{R}.$$

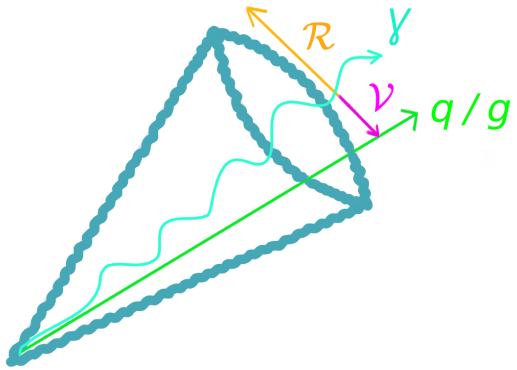

Hybrid-cone isolation: combination of the **smooth**- and **fixed-cone** prescriptions, reduces differences between experiment and theory.

Photons and jets with the ATLAS detector

The ATLAS detector

ATLAS coll., Eur. Phys. J. C **81** (2021) 689

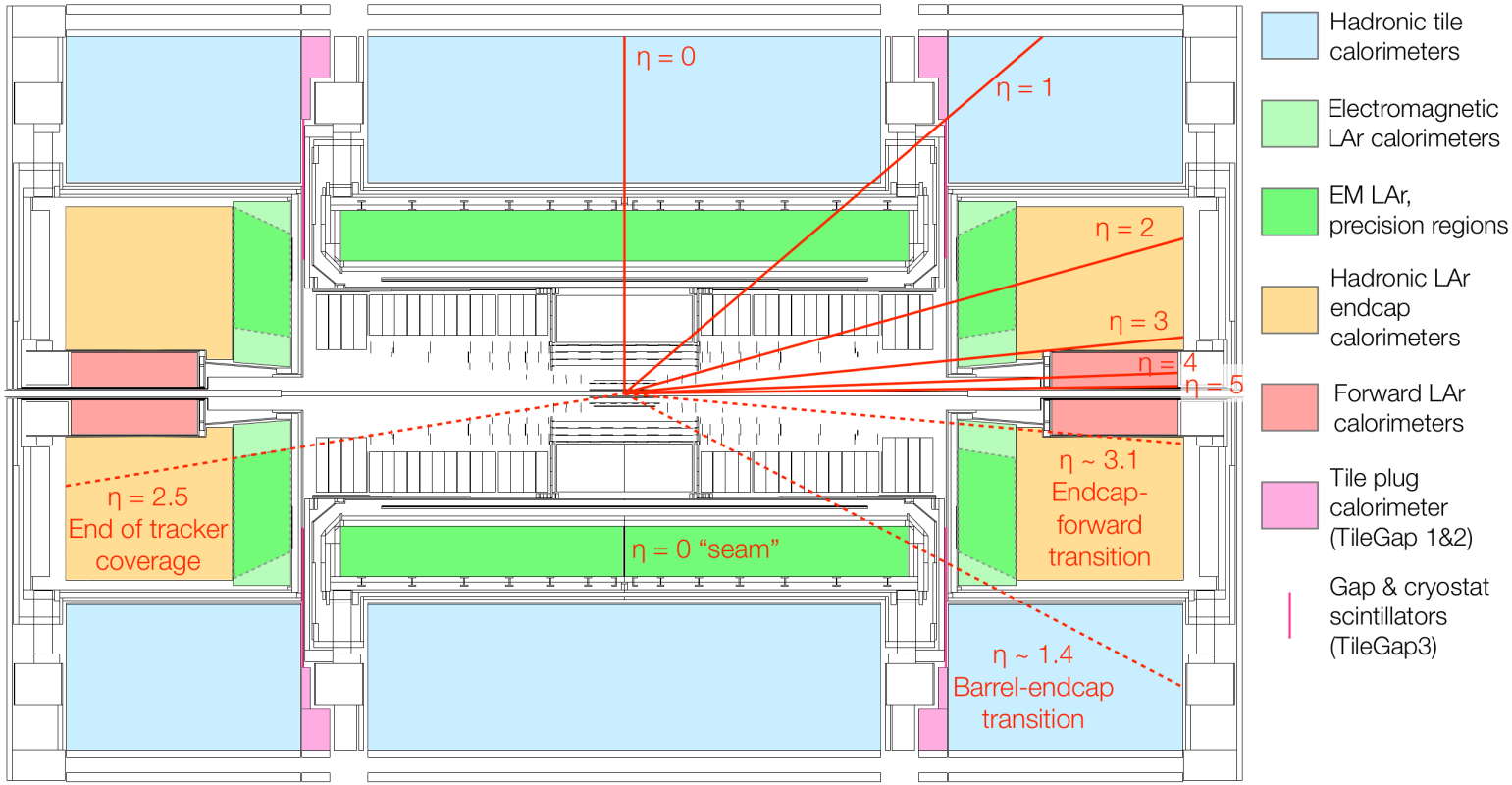

- **Inner detector (silicon pixels, SCT and TRT):** tracking and particle identification in $|\eta| < 2.5$.
- **Calorimeters:** precise measurement of particle energy.

  Electromagnetic (LAr/lead, LAr/Cu): barrel $|\eta| < 1.475$, end-cap $1.375 < |\eta| < 3.2$, forward $3.1 < |\eta| < 4.9$.

  Hadronic (scintillator/steel, LAr/Cu, LAr/W): barrel $|\eta| < 1.0$, extended barrel $0.8 < |\eta| < 1.7$, end-cap $1.5 < |\eta| < 3.2$, forward $3.1 < |\eta| < 4.9$.

Photon reconstruction in ATLAS

Photons are reconstructed from clusters of energy in the electromagnetic (EM) calorimeter. **Three longitudinal layers:**

- **1^{st} layer:** high granularity in the η direction;
- **2^{nd} layer:** collects most of the energy;
- **3^{rd} layer:** used to correct for leakage.

The reconstruction of photons is different for converted and unconverted categories:

- **Unconverted photon candidate:**
  cluster of EM cells without a matching track or conversion vertex in the inner detector.
- **Converted photon candidate:**
  cluster of EM cells matched to a track (or pair of tracks) consistent with originating from a reconstructed photon conversion.

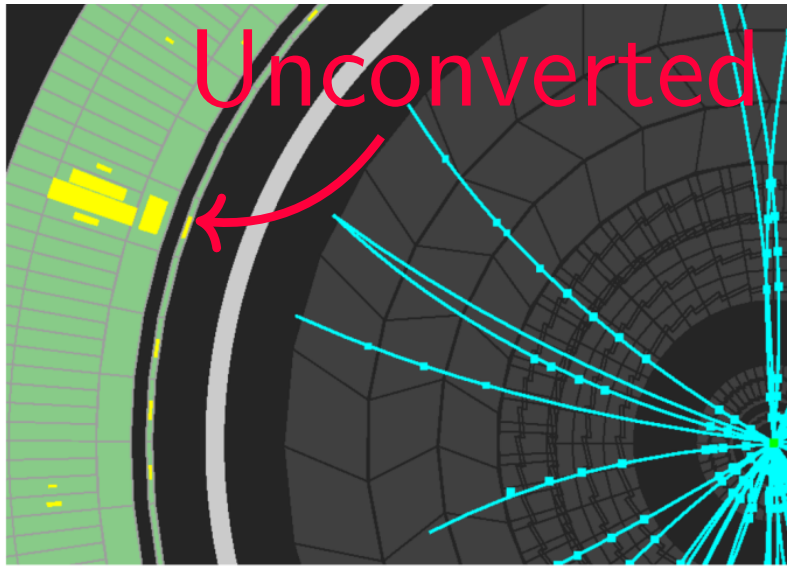

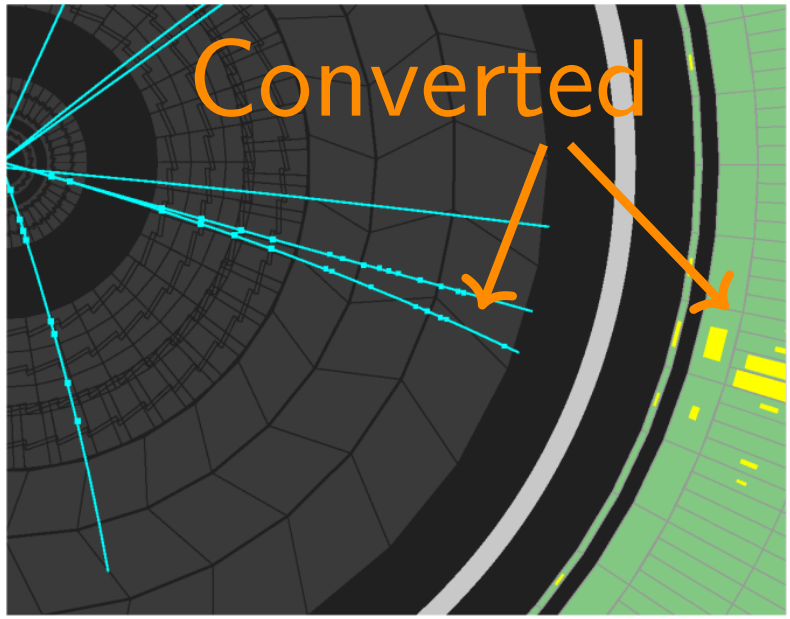

Photon identification in ATLAS

Discrimination between signal and background photons using variables that characterise:

- the lateral/longitudinal shower development in the EM calorimeter;
- the energy fraction leaking into the hadronic calorimeter.

Loose and *tight* identification criteria are used.

- **Loose identification criteria:** discrimination of γ from electrons and hadrons using the 2^{nd} and 3^{rd} layers of LAr and the 1^{st} layer of the hadronic calorimeter.
- **Tight identification criteria:** discrimination of single-γ showers using the 1^{st} layer of the LAr from overlapping nearby showers, such as $\pi^0 \to \gamma\gamma$, in addition to tighter requirements on the shower shapes of the other layers.

  ↪ Additional *loose′* criteria are defined by relaxing some cuts on discriminating variables from the tight criteria.

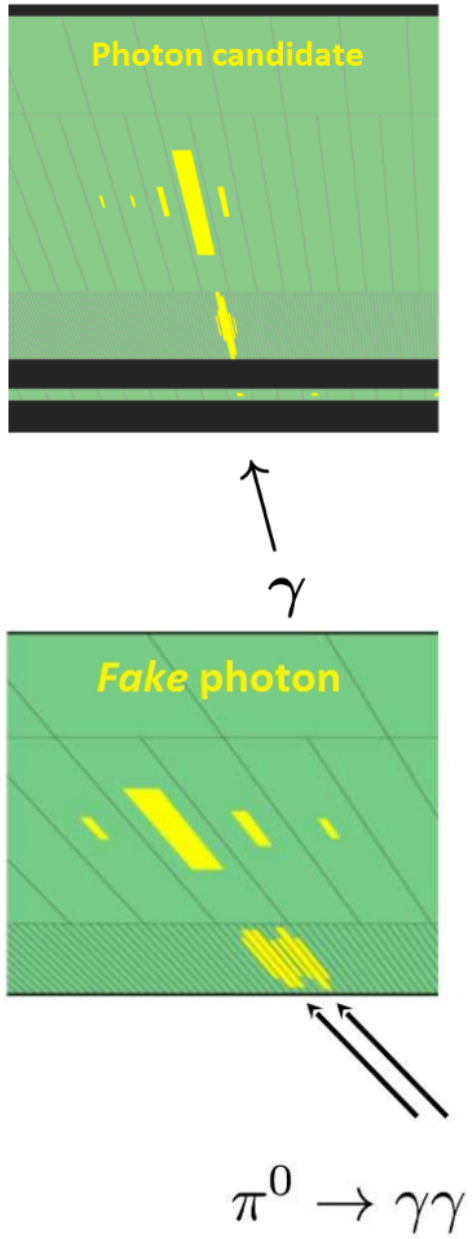

Photon calibration in ATLAS

A precise calibration of the energy measurement of electrons and photons is required for many analyses performed in ATLAS. **The calibration provides:**

- Optimisation of the energy resolution and reduction of the impact of material in front of the calorimeter.
- Adjustment of the relative energy scales of the different layers of the EM calorimeter.
- Correction for residual local non-uniformities in the calorimeter response affecting the data.
- Adjustment of the absolute energy scale and resolution using Z boson decays into e^+e^- pairs.
- Validation of the energy scale universality using J/Ψ decays decays into e^+e^- pairs and radiative Z boson decays.

ATLAS coll., JINST **14** (2019) P12006

Energy scale factors

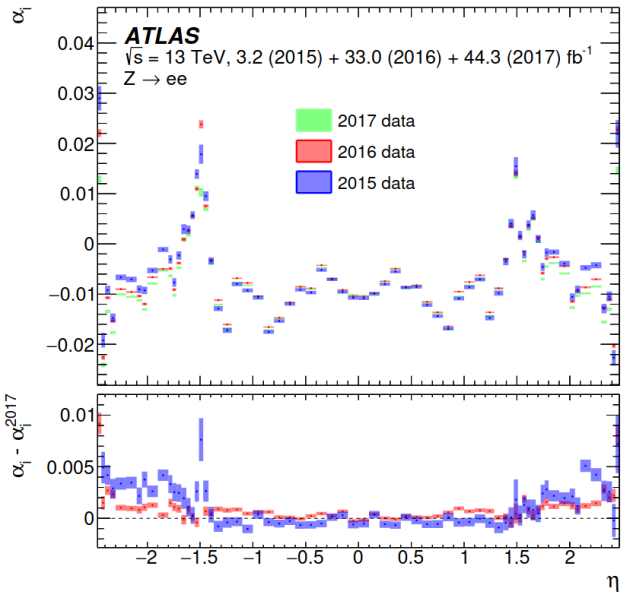

Resolution constant term

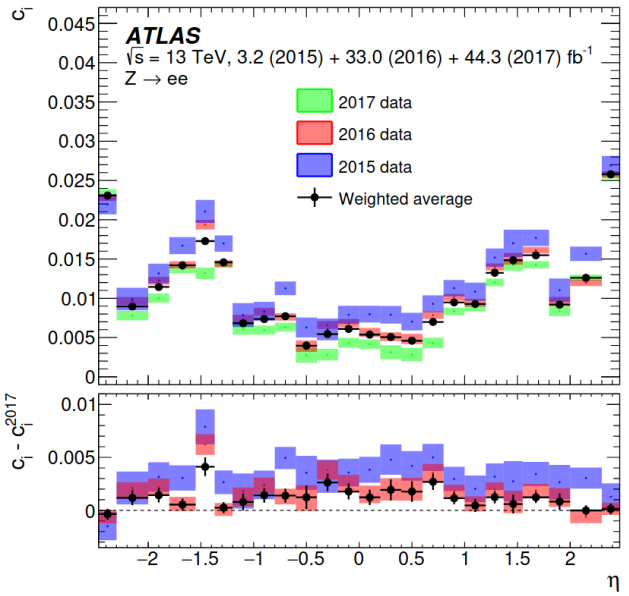

Photon isolation in ATLAS

The isolation transverse energy ($E_{\mathrm{T}}^{\mathrm{iso}}$) is computed at detector level using clusters of calorimeter cells (EM and hadronic) in a cone of radius R, excluding an area centred on the photon cluster.

Corrections applied:

– for the expected leakage of the photon energy into the isolation cone (few %);

– for the underlying event (UE) and pile-up contributions to $E_{\mathrm{T}}^{\mathrm{iso}}$ using the jet-area method.

A photon candidate is considered isolated if the condition $E_{\mathrm{T}}^{\mathrm{iso}} < E_{\mathrm{T,cut}}^{\mathrm{iso}}$ is fulfilled.

→ Residual background is still expected even after tight identification and isolation requirements.

Jet-area method (M. Cacciari et al., JHEP **04** (2010) 065)

Isolation distributions (ATLAS-CONF-2022-065)

Cone of $R = 0.2$

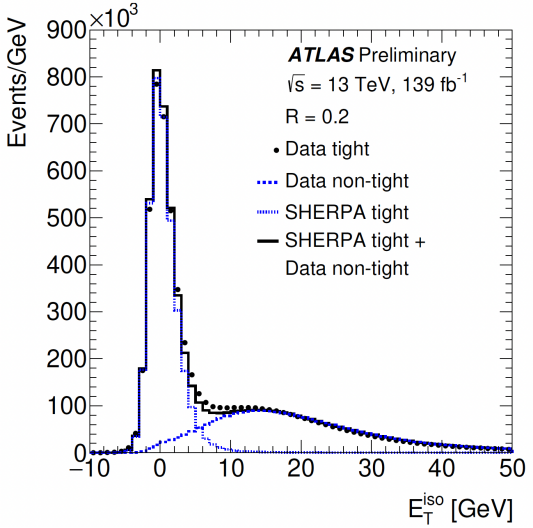

Cone of $R = 0.4$

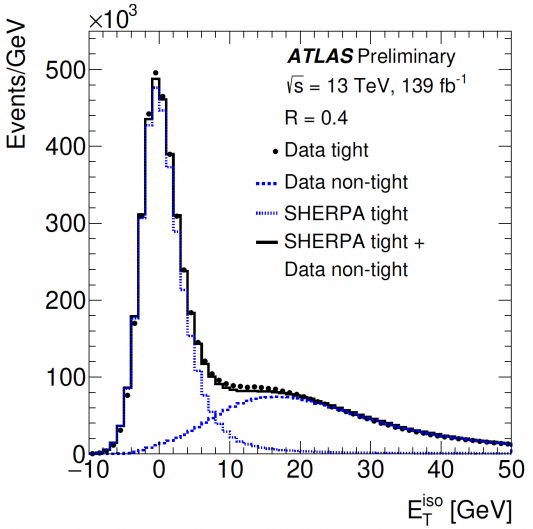

Background subtraction

Residual background contribution from jets misidentified as photons:

- Bin-by-bin evaluation using a data-driven technique based on the plane defined by the γ_{ID} and $E_{\mathrm{T}}^{\mathrm{iso}}$ variables.
- Leading loose′ photon classified into one of the four regions in the plane:
  B, C and D: background control regions;
  A: signal region.

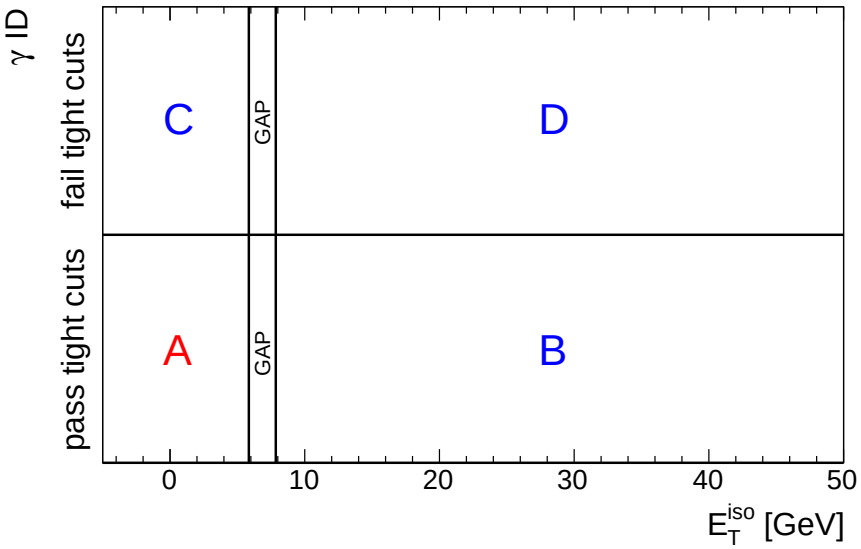

The signal yield ($N_{\mathrm{A}}^{\mathrm{sig}}$) in region A is extracted with:

$$N_{\mathrm{A}}^{\mathrm{sig}} = N_{\mathrm{A}} - R^{\mathrm{bg}} \frac{(N_{\mathrm{B}} - \epsilon_{\mathrm{B}} N_{\mathrm{A}}^{\mathrm{sig}})(N_{\mathrm{C}} - \epsilon_{\mathrm{C}} N_{\mathrm{A}}^{\mathrm{sig}})}{(N_{\mathrm{D}} - \epsilon_{\mathrm{D}} N_{\mathrm{A}}^{\mathrm{sig}})} .$$

No correlation between γ_{ID} and $E_{\mathrm{T}}^{\mathrm{iso}}$ is assumed for background events:

$$R^{\mathrm{bg}} \equiv \frac{N_{\mathrm{A}}^{\mathrm{bg}} N_{\mathrm{D}}^{\mathrm{bg}}}{N_{\mathrm{B}}^{\mathrm{bg}} N_{\mathrm{C}}^{\mathrm{bg}}} = 1 .$$

Signal leakage fractions (ϵ_{K}) from MC:

$$\epsilon_{\mathrm{K}} = N_K^{\mathrm{sig}} / N_A^{\mathrm{sig}} .$$

Jet reconstruction

- **Primary jet definition in ATLAS: anti-k_t algorithm with $R = 0.4$.**
- **Various objects are used as inputs to the algorithm:**
  - Stable particles defined by MC generators (**truth jets**).
  - Charged particle tracks (**track jets**).
  - Calorimeter energy deposits (**EM jets**):

    Jets reconstructed with clusters defined at the EM scale.
  - Algorithmic combinations of calorimeter deposits and tracks (**PFlow jets**):

    Energy depositions by charged particles are subtracted from the clusters and replaced by the momentum of matched tracks.

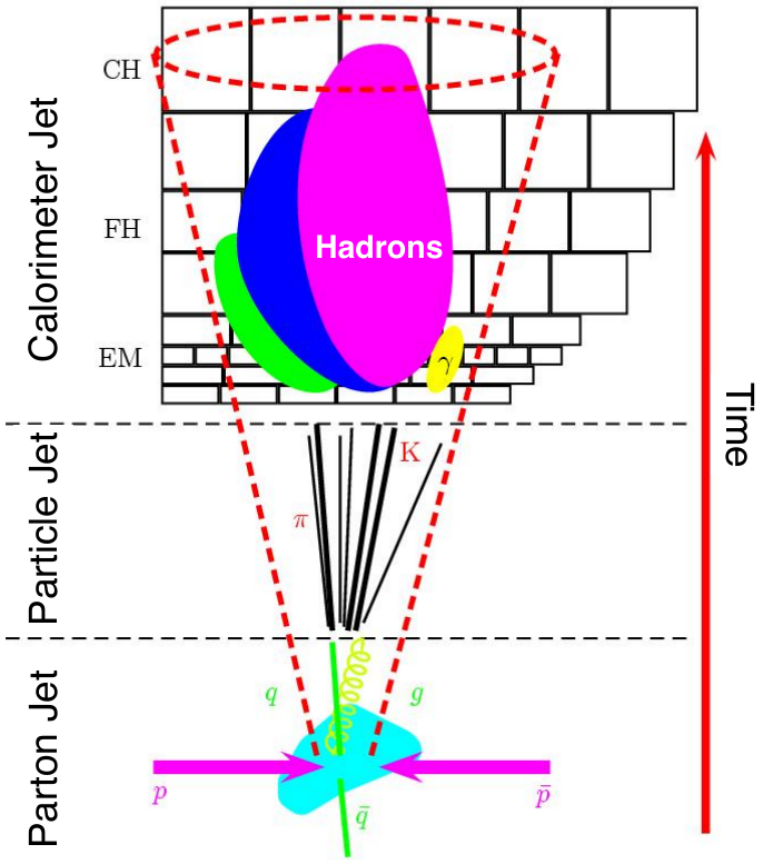

- **Origin correction:** corrects the cluster 4-momentum to point to the primary vertex of the hard scattering.

Jet calibration

After reconstruction, jets are calibrated to the energy scale of truth jets to compensate for detector- and reconstruction-based limitations.

Jet Energy Scale calibration (JES):

- Pile-up corrections: remove the excess energy due to pile-up.
- Absolute MC-based calibration: corrects the jet so that it agrees in energy and η with truth jets
- Global sequential calibration: improves the jet p_{T} resolution.
- Residual in situ calibration: corrects for remaining differences between data and MC.

All stages correct the jet four-momentum.

The **Jet Energy Resolution (JER)** is also calibrated in situ with the dijet balance and noise term measurements.

Absolute MC-based calibration

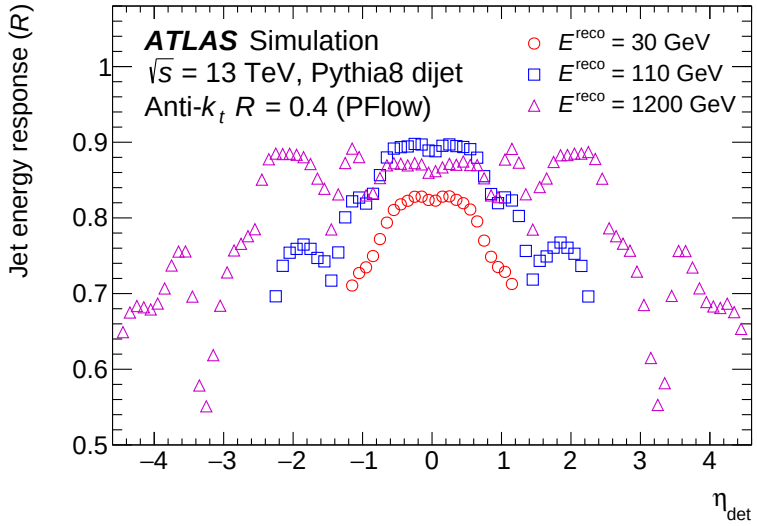

JER calibration

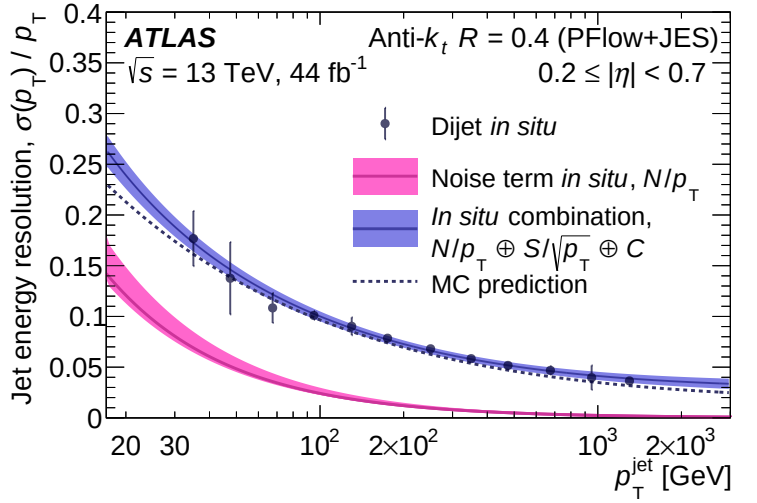

ATLAS coll., Eur. Phys. J. C **81** (2021) 689

Perturbative QCD theoretical calculations

Monte Carlo simulations

The MC generators PYTHIA 8.186 and SHERPA 2.1.1 were used to simulate signal events.

PYTHIA:

- LO γ+jet events from direct processes and photon bremsstrahlung in LO QCD dijet events.
- Fragmentation into hadrons: Lund-string model.

SHERPA:

- LO matrix elements for γ+jet events with up to 3 additional partons $(2 \to 5)$.
- Fragmentation into hadrons: Cluster model.

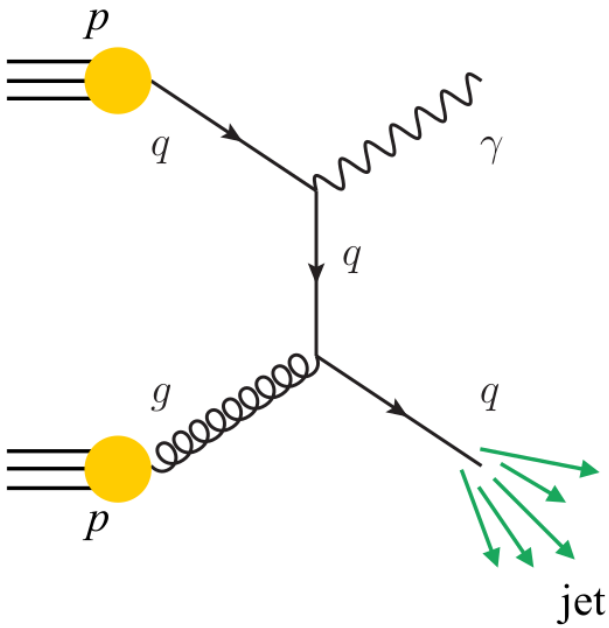

$pp \to \gamma + \text{jet} + \text{X}$

Both MC programs are supplemented with parton showers and contain simulations for UE and pile-up.

Samples generated at particle and detector levels: study the characteristics of signal events, unfolding corrections and hadronisation and UE corrections.

T. Sjöstrand et al., Comput. Phys. Commun. **178** (2008) 852

T. Gleisberg et al., JHEP **02** (2009) 007

NLO pQCD predictions: JETPHOX

JETPHOX 1.3.1_2 provides full fixed-order NLO pQCD predictions for direct and fragmentation contributions:

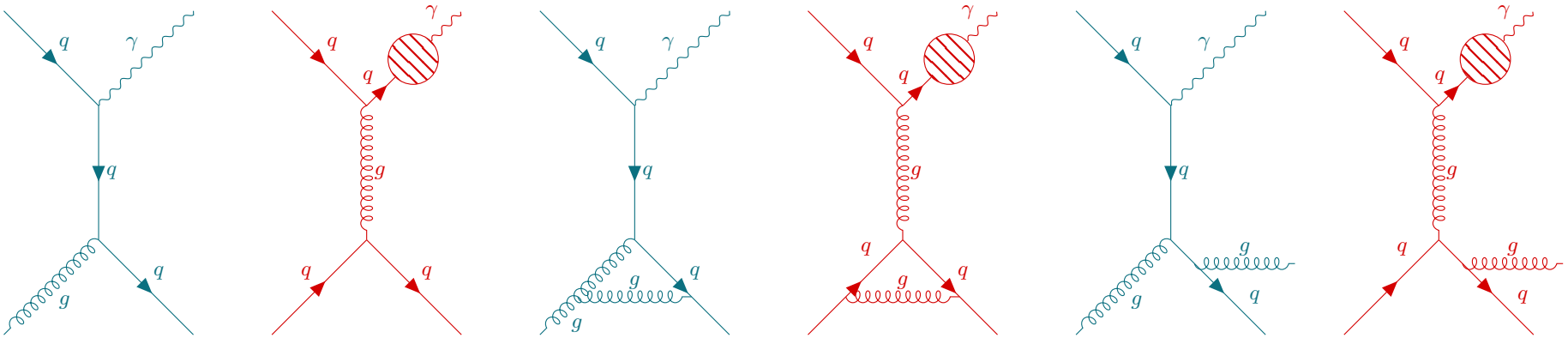

$$\sigma_{pp\to\gamma+X} = \sum_{i,j,a} \int_0^1 dx_i\, f_i\left(x_i, \mu_F^2\right) \int_0^1 dx_j\, f_j\left(x_j, \mu_F^2\right)\, \hat{\sigma}_{ij\to\gamma a}$$

$$+ \sum_{i,j,a,b} \int_0^1 dx_i\, f_i\left(x_i, \mu_F^2\right) \int_0^1 dx_j\, f_j\left(x_j, \mu_F^2\right) \int_{z_{\min}}^1 dz\, D_\gamma^a\left(z, \mu_f^2\right)\, \hat{\sigma}_{ij\to ab}$$

- **Scales:** $\mu_{\mathrm{R}} = \mu_{\mathrm{F}} = \mu_{\mathrm{f}} = E_{\mathrm{T}}^{\gamma}/2$ or E_{T}^{γ}.
- **Photon fragmentation functions:** BFG set II.
- **Predictions for several PDFs:** MMHT2014, CT18, NNPDF3.1, ...
- **Fixed-cone isolation** implemented at parton level.
- **Non-perturbative corrections:** $\lesssim 1\%$ for inclusive photon production.

S. Catani et al., JHEP **05** (2002) 028

NLO pQCD predictions: SHERPA NLO

SHERPA 2.2.2 (SHERPA NLO) includes parton-level calculations for γ+1,2 (3,4) jets at NLO (LO) supplemented with parton shower:

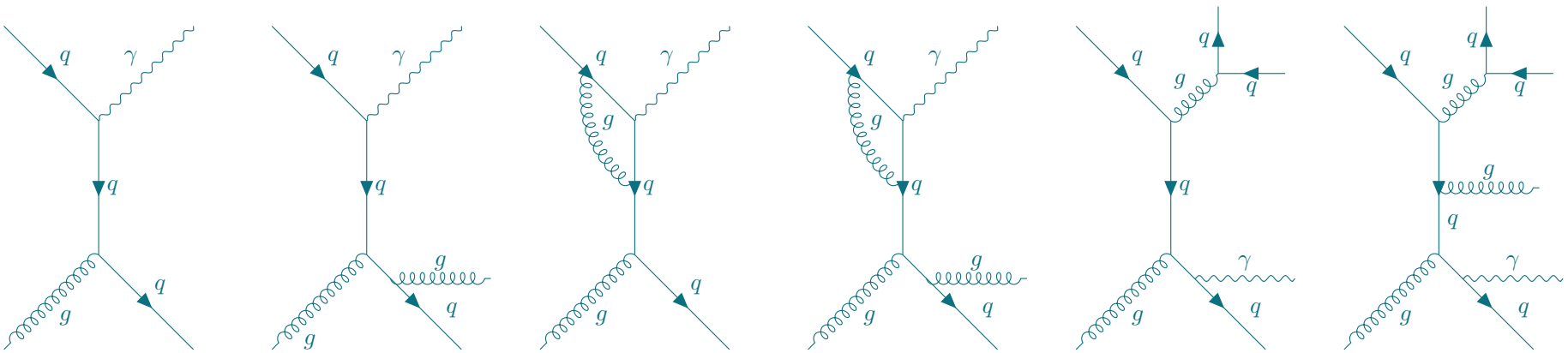

$$\sigma_{pp\to\gamma+X} = \sum_{i,j,a} \int_0^1 dx_i \, f_i\left(x_i, \mu_F^2\right) \int_0^1 dx_j \, f_j\left(x_j, \mu_F^2\right) \, \hat{\sigma}_{ij\to\gamma a}$$

- Only direct contribution (**Frixione's isolation** at matrix-element level).
- **Scales:** dynamic setting (E_{T}^{γ}).
- **PDF set:** NNPDF3.0 NNLO.
- **Fragmentation into hadrons and UE** simulated as for SHERPA 2.1.1.
- **Fixed-cone isolation** implemented at particle level.

E. Bothmann et al., SciPost Phys. **7** (2019) 034

NNLO pQCD predictions: NNLOJET

The NNLOJET framework provides fixed-order NNLO pQCD predictions for direct and fragmentation contributions:

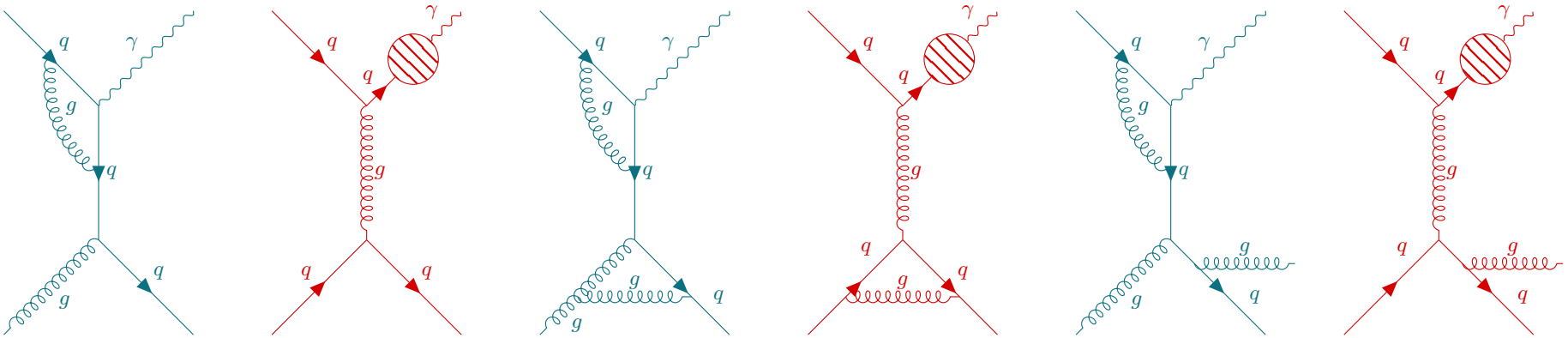

$$\sigma_{pp\to\gamma+X} = \sum_{i,j,a} \int_0^1 dx_i\, f_i\left(x_i, \mu_F^2\right) \int_0^1 dx_j\, f_j\left(x_j, \mu_F^2\right)\, \hat{\sigma}_{ij\to\gamma a}$$

$$+ \sum_{i,j,a,b} \int_0^1 dx_i\, f_i\left(x_i, \mu_F^2\right) \int_0^1 dx_j\, f_j\left(x_j, \mu_F^2\right) \int_{z_{\min}}^1 dz\, D_\gamma^a\left(z, \mu_f^2\right)\, \hat{\sigma}_{ij\to ab}$$

- **Scales:** $\mu_{\mathrm{R}} = \mu_{\mathrm{F}} = E_{\mathrm{T}}^{\gamma}$, and $\mu_{\mathrm{f}} = \sqrt{E_{\mathrm{T}}^{\gamma} \cdot E_{\mathrm{T}}^{\mathrm{max}}} \cdot R$.
- **Photon fragmentation functions:** BFG set II.
- **PDF set:** CT18 NNLO.
- **Fixed-cone isolation** implemented at parton level.
- **Non-perturbative corrections:** same estimation as for JETPHOX.

X. Chen et al., JHEP **08** (2022) 094

Theoretical uncertainties

Theoretical uncertainties are evaluated for the pQCD predictions of JETPHOX, SHERPA NLO and NNLOJET:

- **Scale variations:** estimated varying the scales $\times 0.5$ or $\times 2$ singly or simultaneously.
- **PDFs:** estimated for JETPHOX (SHERPA NLO) using the 50 sets (100 replicas) from the MMHT2014 (NNPDF3.0) error analysis.
- α_S**:** evaluated using two additional sets of PDFs for which different values of $\alpha_S\left(M_Z^2\right)$ are assumed.
- **Non-perturbative corrections:** evaluated with PYTHIA by computing the factor

$$C_{\mathrm{NP}} = \sigma^{\mathrm{particle,UE}} / \sigma^{\mathrm{parton,no-UE}} \quad .$$

Consistent with unity within $\pm 1\%$ (1% uncertainty assigned).

ATLAS-CONF-2022-065

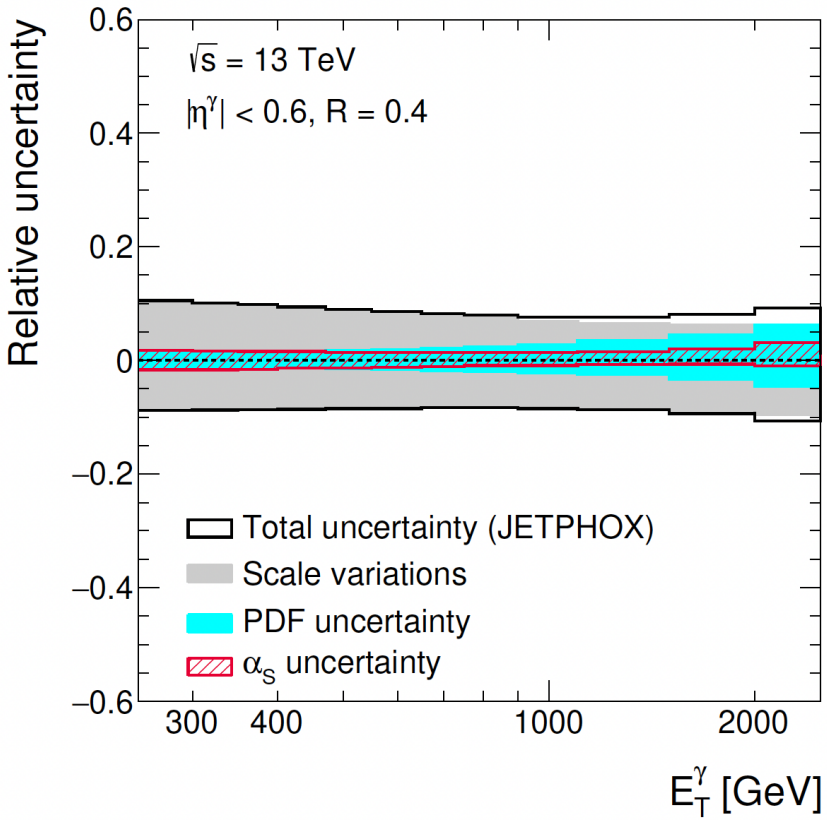

→ **Total uncertainty estimated by adding in quadrature the individual contributions listed above.**

Inclusive photon at 13 TeV using the full Run-2 ATLAS data

Conference note: ATLAS-CONF-2022-065

Event and object selection

Measurement of the inclusive isolated-photon cross section in pp collisions at $\sqrt{s} = 13$ TeV using the full Run-2 data.

- The $\mathrm{d}\sigma/\mathrm{dE}_{\mathrm{T}}^{\gamma}$ were measured as a function of E_{T}^{γ} in six $|\eta^{\gamma}|$ regions:

Previous $[0.0, 0.6, 1.37, 1.56, 1.81, 2.37]$

New $[0.0, 0.6, 0.8, 1.37, 1.56, 1.81, 2.01, 2.37]$

- Photons with $E_{\mathrm{T}}^{\gamma} > 250$ GeV and $|\eta^{\gamma}| < 2.37$ (excluding $1.37 < |\eta^{\gamma}| < 1.56$).

- Tight identification and isolation:

$$E_{\mathrm{T,cut}}^{\mathrm{iso}} = 4.2 \times 10^{-3} \times E_{\mathrm{T}}^{\gamma} + 4.8 \text{ GeV}.$$

- $\mathrm{d}\sigma/\mathrm{dE}_{\mathrm{T}}^{\gamma}$ measured for two γ-isolation cone sizes: $R = 0.2$ and $R = 0.4$.

↪ Test the R-dependence of the inclusive photon cross sections at 13 TeV.

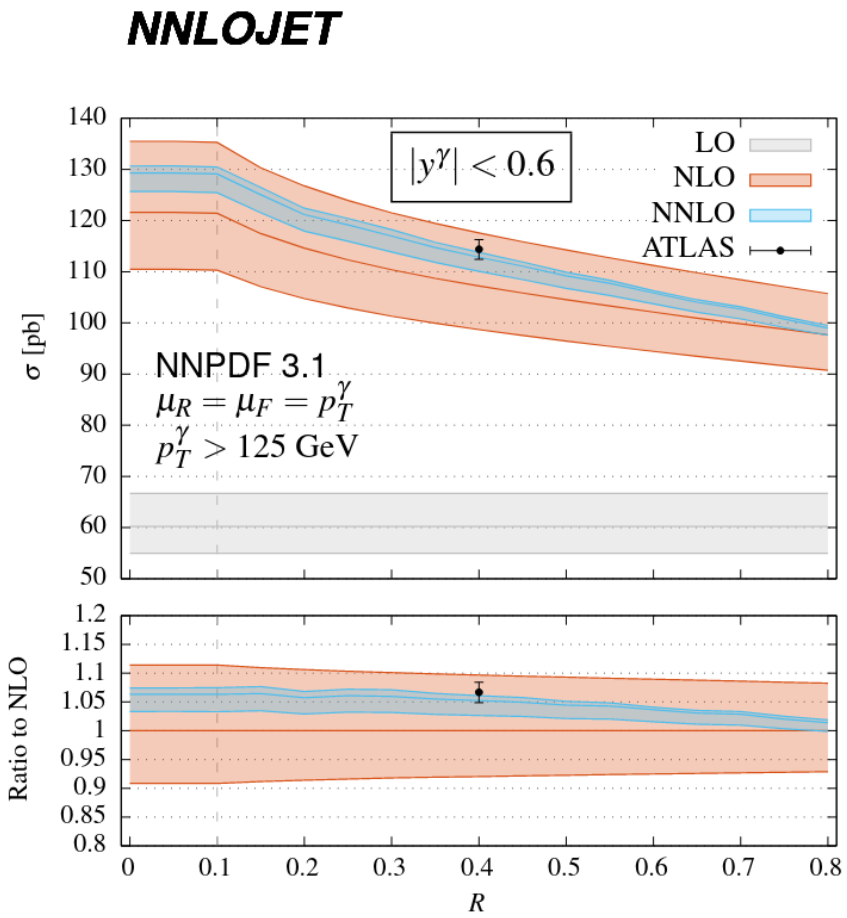

X. Chen et al., JHEP **04** (2020) 166

Signal purity

- Background subtracted with the ABCD method using signal leakage fractions from SHERPA.

  ↪ Slightly larger differences between SHERPA and PYTHIA for $R = 0.2$.

- The signal purity was calculated using

$$P = \frac{N_{\mathrm{A}}^{\mathrm{sig}}(i)}{N_{\mathrm{A}}(i)}.$$

  – Greater than 93% and slightly higher for $R = 0.4$ compared to $R = 0.2$.

  – Similar $N_{\mathrm{A}}^{\mathrm{sig}}(i)$ estimation using either SHERPA or PYTHIA signal leakage fractions.

  ↪ Differences taken as a systematic uncertainty (effect on the cross section typically $< 0.5\%$).

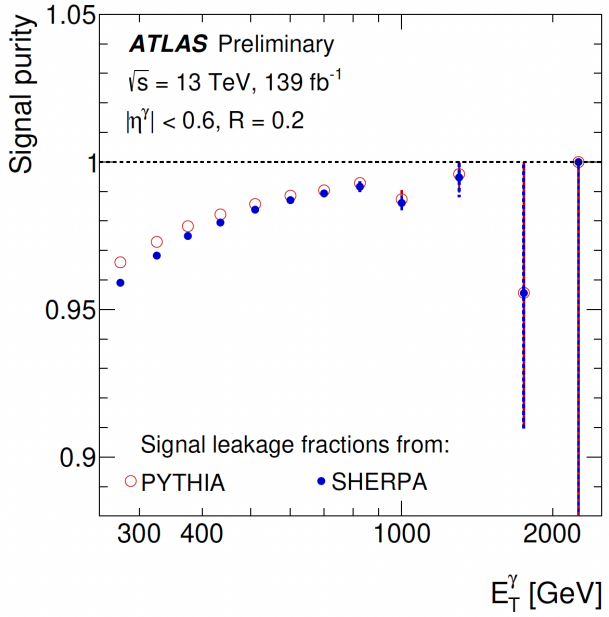

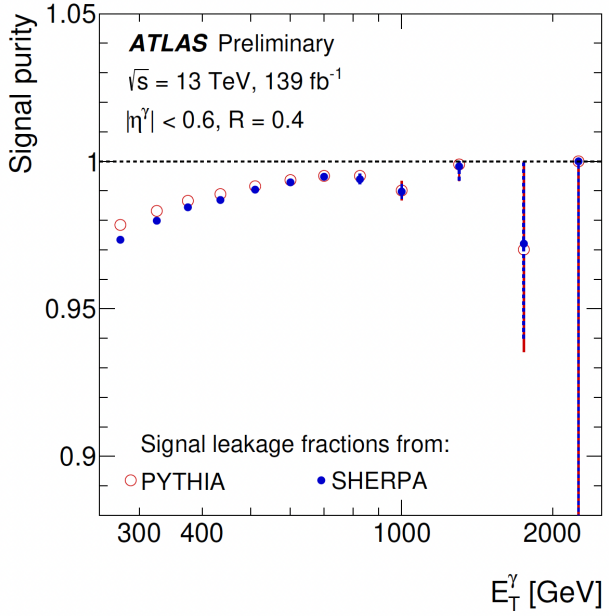

ATLAS-CONF-2022-065

Unfolding correction

- **The cross section was measured with the Bayes method, and the bin-by-bin method was used as a cross-check:**
  - RooUnfold was used in each $|\eta^{\gamma}|$ region with two iterations.
  - Unfolding matrix, unmatched fractions and Bayes vs bin-by-bin cross sections:

$\rightarrow$ Isolation cone $R = 0.2$

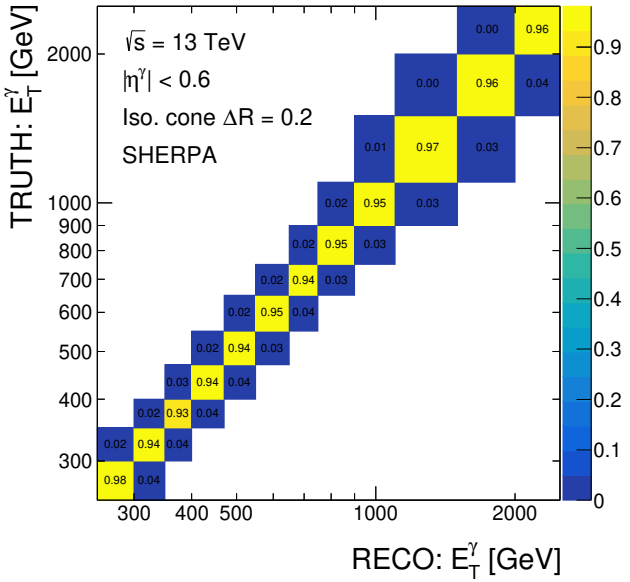

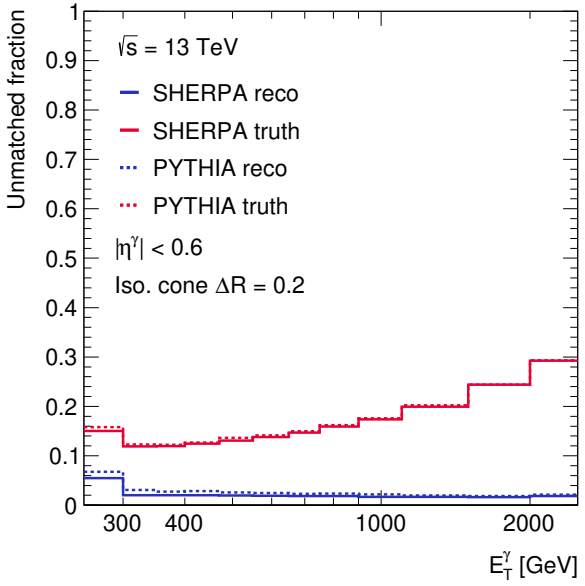

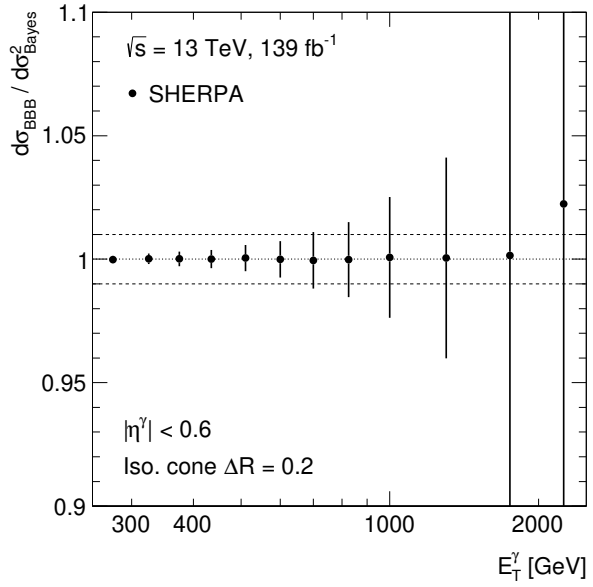

$\rightarrow$ **Bayes vs bin-by-bin:** differences typically **much smaller** than $1\,\%$ due to the very diagonal unfolding matrices.

CERN-THESIS-2021-240

Systematic uncertainties

- **Signal modelling:**
  - Signal leakage fractions from PYTHIA
- **Background subtraction:**
  - Choice of background control regions
  - **Identification and isolation correlation in the background (R^{bg})**
  - Background from electrons faking photons
- **Photon reconstruction:**
  - Photon reconstruction efficiency
  - **Photon identification efficiency**
  - $E_{\mathrm{T}}^{\mathrm{iso}}$ modelling
- **Unfolding procedure:**
  - Unfolding with PYTHIA
  - Unfolding closure
  - MC statistical uncertainty
- **Running conditions:**
  - **Pile-up**
  - Uncertainty on the trigger efficiency
  - Luminosity-measurement uncertainty ($1.7\,\%$)
- **Photon calibration:**
  - **Photon energy scale** and resolution

Photon identification uncertainty

- Uncertainty on the photon identification efficiency.
  - Nominal cross section calculated applying scale factors to MC samples.
  - Uncertainties of the scale factors were propagated to estimate the systematic uncertainty.

    ↪ Effect on the cross section: $0.5\% - 0.75\%$.
  - Large reduction of this uncertainty with respect to the previous analysis at 13 TeV using $36.1\ \mathrm{fb}^{-1}$ of the Run-2 luminosity:

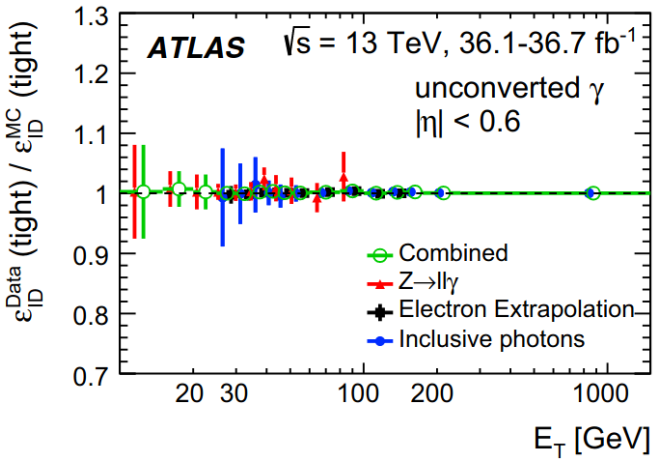

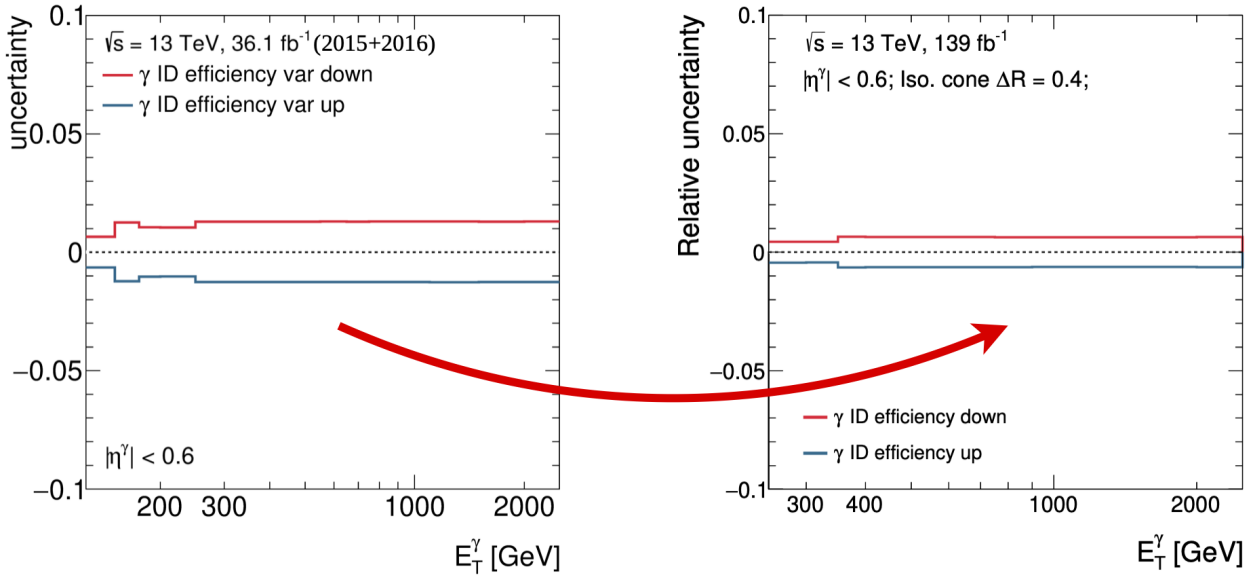

CERN-THESIS-2021-240

ATLAS coll., Eur. Phys. J. C **79** (2019) 205

R^{bg} uncertainty

- The correlation R^{bg} was studied in background events using a data-driven method.
  - The nominal cross section is calculated using $R^{\mathrm{bg}} = 1$.
  - Uncertainty in R^{bg} taken as the largest deviation of R^{bg} from unity obtained from the results using either PYTHIA or SHERPA.
  - Systematic uncertainty varying R^{bg} up/down in the range obtained from the study (0.75 to 1.25).
    - ↪ Effect on the cross section: $\lesssim 2\%$, and typically $< 1\%$.

$R = 0.2$

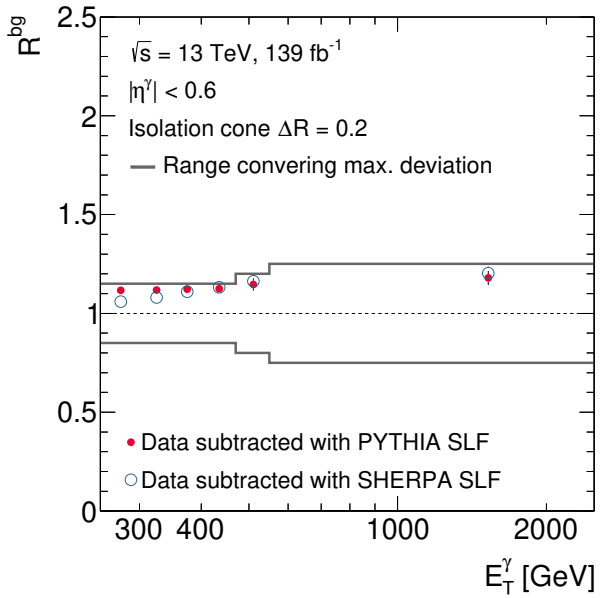

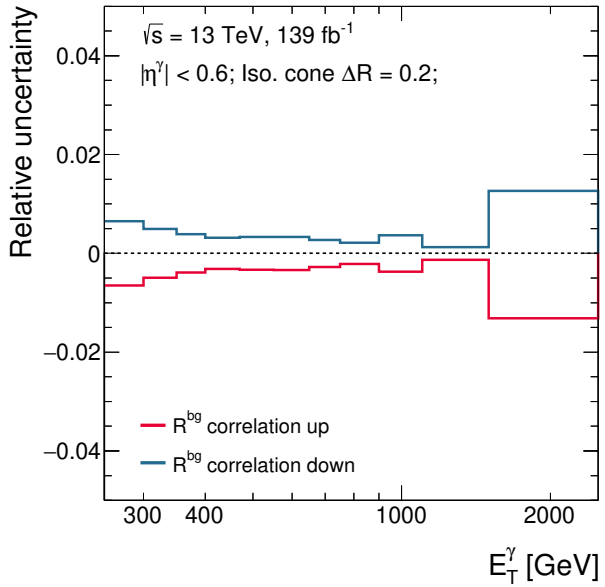

CERN-THESIS-2021-240

Pile-up uncertainty

$R = 0.2$

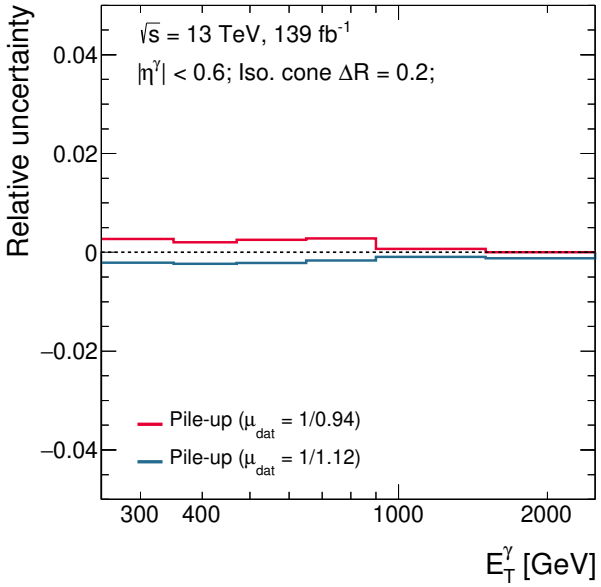

$R = 0.4$

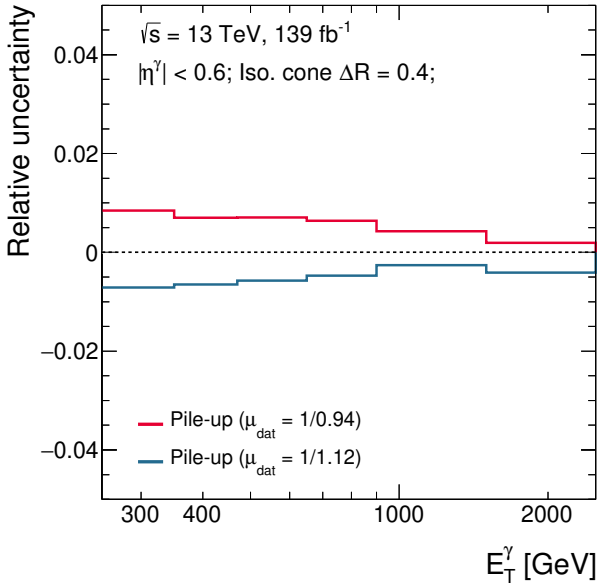

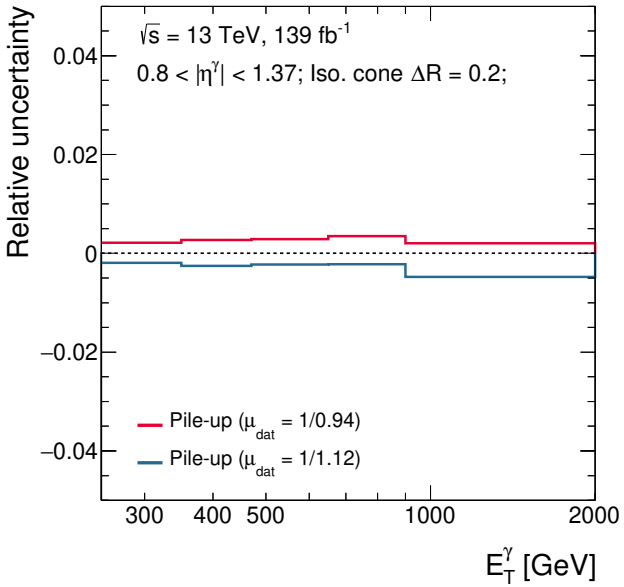

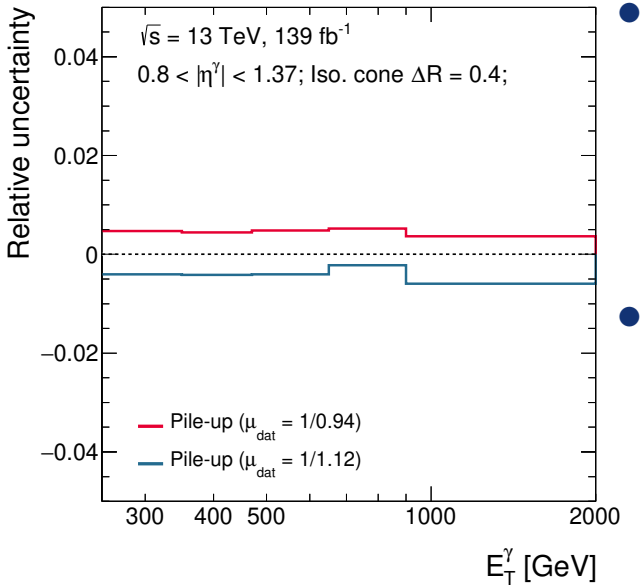

- For the nominal cross section calculation, the MC $\langle\mu\rangle$ distribution was reweighted to that of the data after applying a factor of $1/1.03$.
- To estimate the systematic uncertainty, the factor applied to the data was changed to $1/0.94$ or $1/1.12$.
- This uncertainty is significantly smaller for $R = 0.2$ compared to $R = 0.4$.
- Effect on the cross section: $\lesssim 1\%$ (1.5%) for $R = 0.2$ $(R = 0.4)$.

CERN-THESIS-2021-240

Photon energy scale uncertainty

- **Uncertainty evaluation:**

  The full decomposition model provided by the ATLAS Combined Performance group of electrons and photons (69 NP) was used.

  – Each of the 69 NP was varied separately in SHERPA to estimate each systematic uncertainty.

  – A smoothing procedure was applied to each of the 69 individual components.

- **Total GES uncertainty estimation:**

  The smoothed results of the 69 individual components are added in quadrature.

  ↪ Effect on the cross section: $1\% - 20\%$, showing no dependence on R.

$R = 0.2$

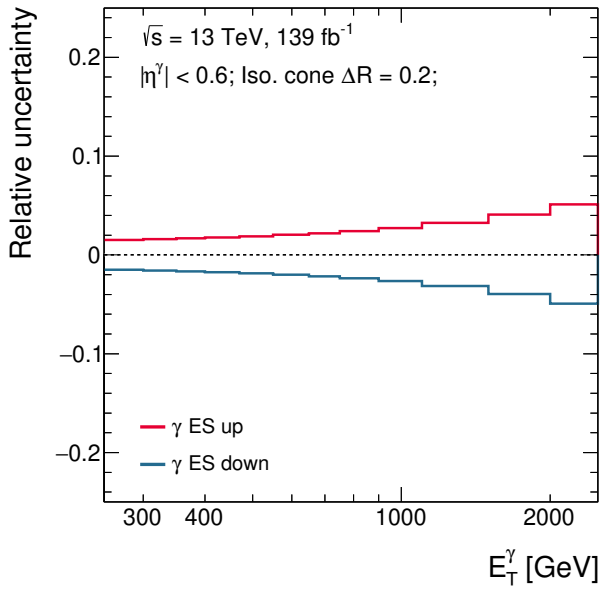

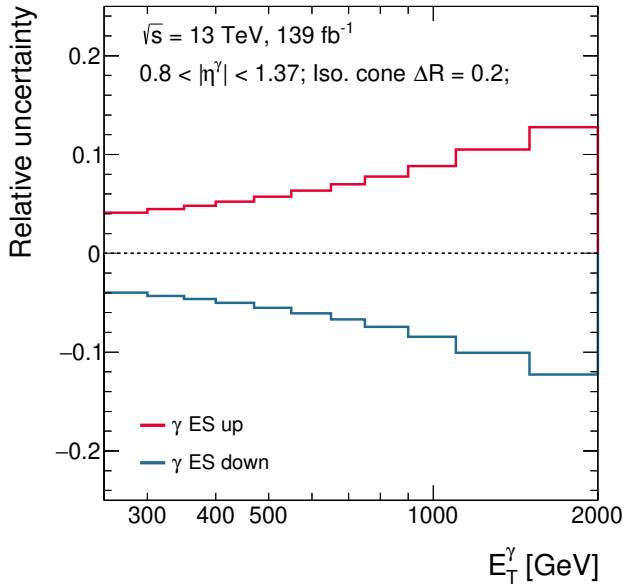

CERN-THESIS-2021-240

Dominant systematic uncertainties

$\rightarrow$ Isolation cone $\mathrm{R} = 0.2$

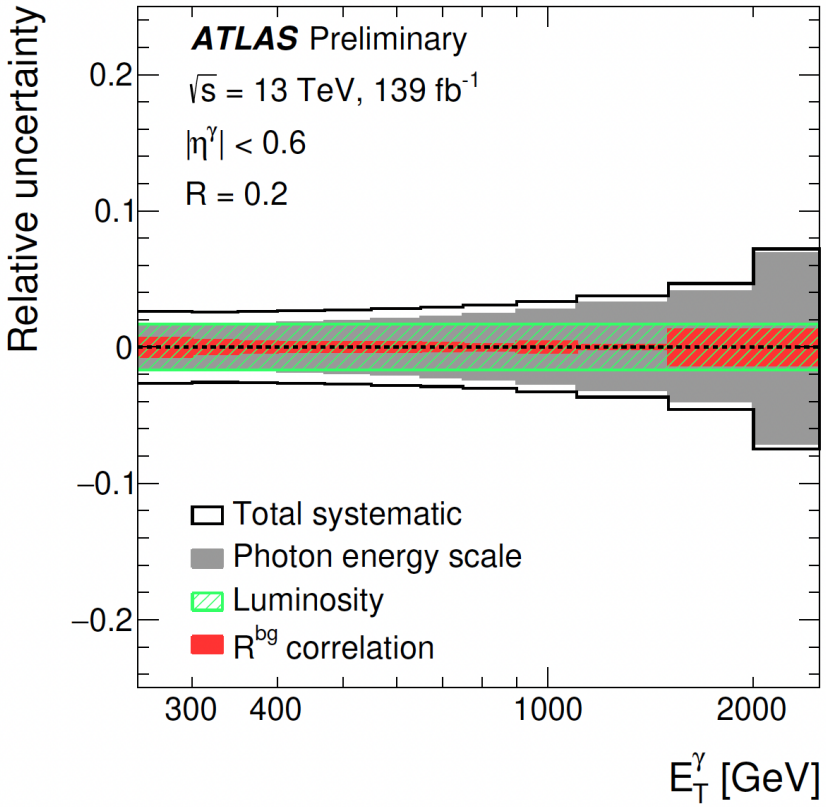

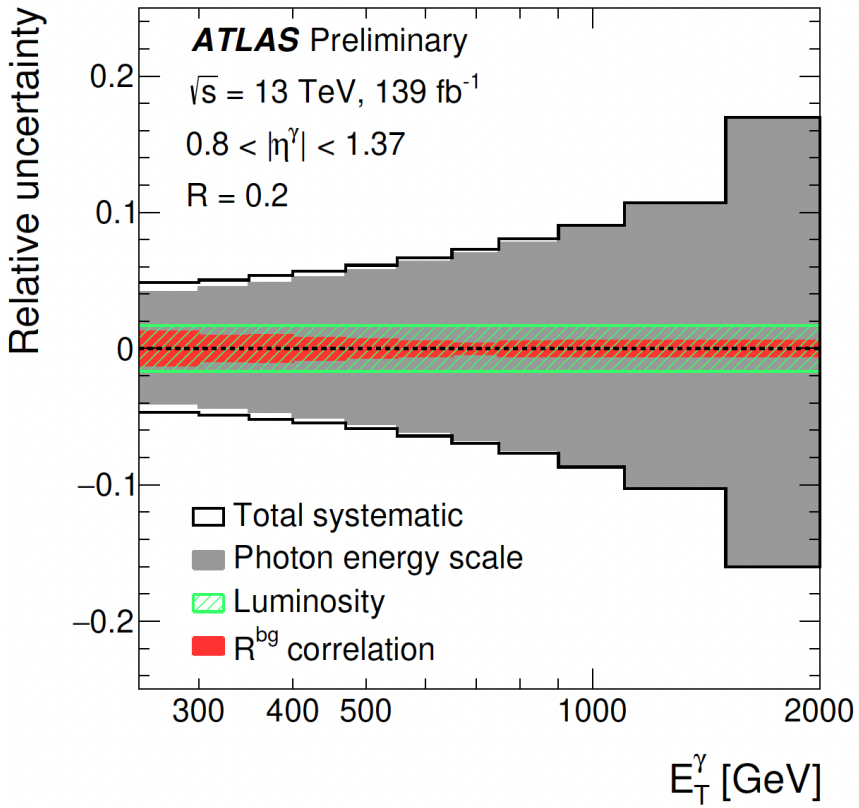

ATLAS-CONF-2022-065

- The uncertainty due to the photon energy scale is dominant: values $2\% - 17\%$ $(3\% - 20\%)$ are reached for $|\eta^{\gamma}| < 1.37$ $(|\eta^{\gamma}| > 1.56)$.
- The uncertainty due to the luminosity (1.7%) dominates at low E_{T}^{γ}.
- The uncertainty due to the R^{bg} correlation represents an important contribution at low and medium E_{T}^{γ}: $0.5\% - 2\%$.

Dominant systematic uncertainties

$\rightarrow$ Isolation cone $\mathrm{R} = 0.4$

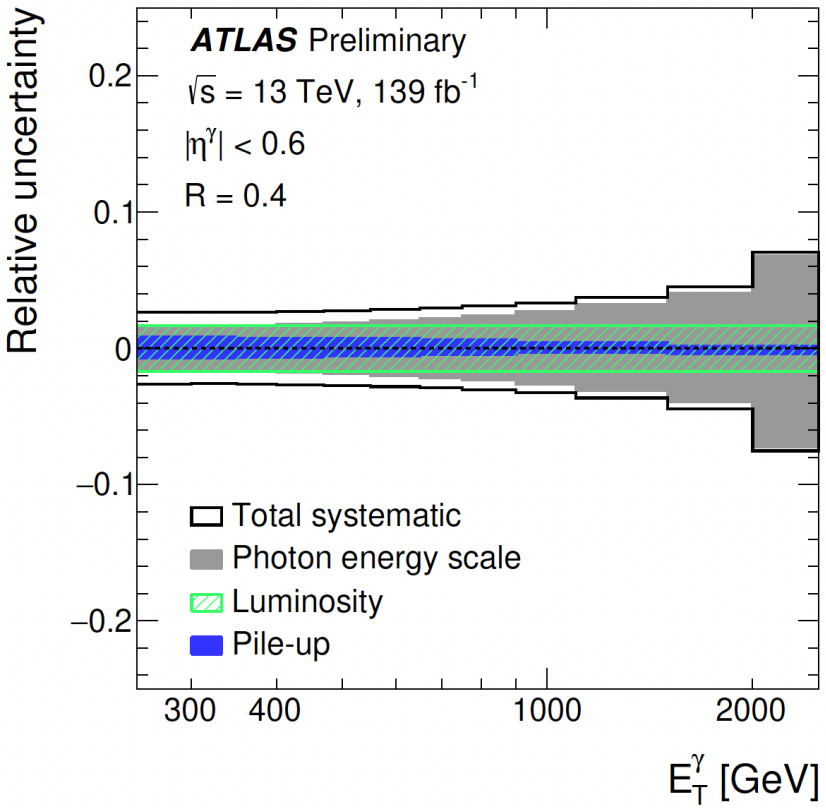

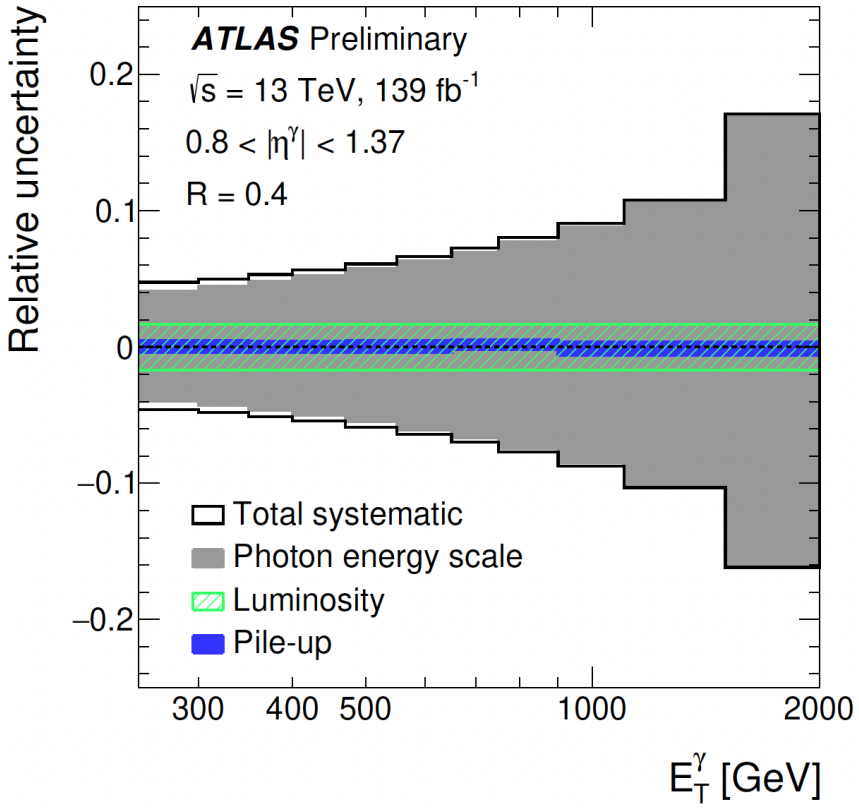

ATLAS-CONF-2022-065

- The uncertainty due to the photon energy scale is dominant: values $2\% - 17\%$ $(3\% - 20\%)$ are reached for $|\eta^{\gamma}| < 1.37$ $(|\eta^{\gamma}| > 1.56)$.
- The uncertainty due to the luminosity (1.7%) dominates at low E_{T}^{γ}.
- The uncertainty due to pile-up represents an important contribution at low and medium E_{T}^{γ}: $0.5\% - 1.5\%$.

Differential cross sections

- The NLO pQCD predictions of SHERPA and JETPHOX, and the NNLO pQCD predictions of NNLOJET compared to the measurements for the two different R values measured.

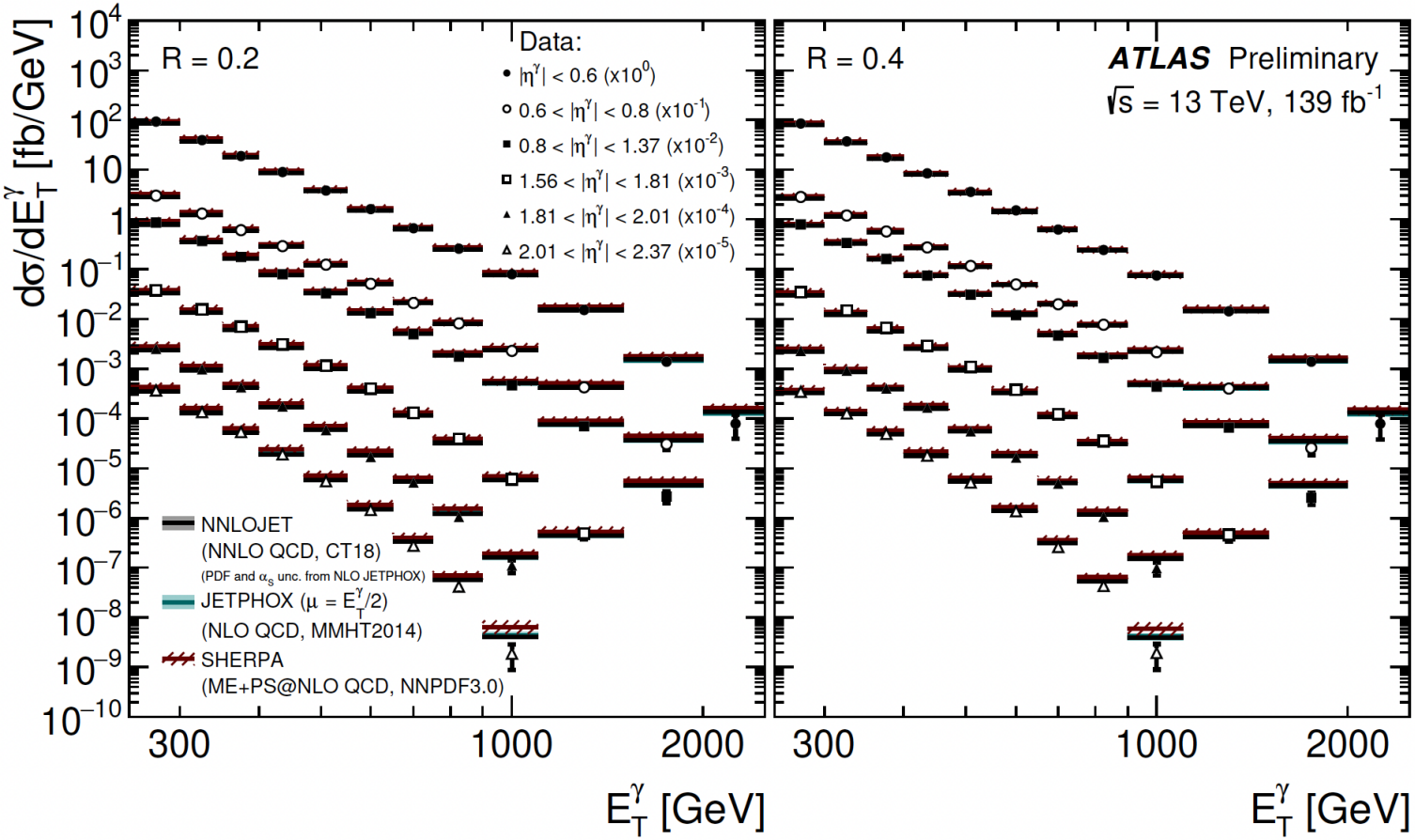

ATLAS-CONF-2022-065

→ **These predictions are consistent with each other within uncertainties**

Differential cross sections: data vs JETPHOX

- The measured cross sections compared to the NLO pQCD predictions of JETPHOX as a function of E_{T}^{γ} in the different $|\eta^{\gamma}|$ regions.

→ **Several PDFs compared:** MMHT2014, CT18, NNPDF3.1, HERAPDF2.0, and ATLASpdf21.

Results with $R = 0.2$

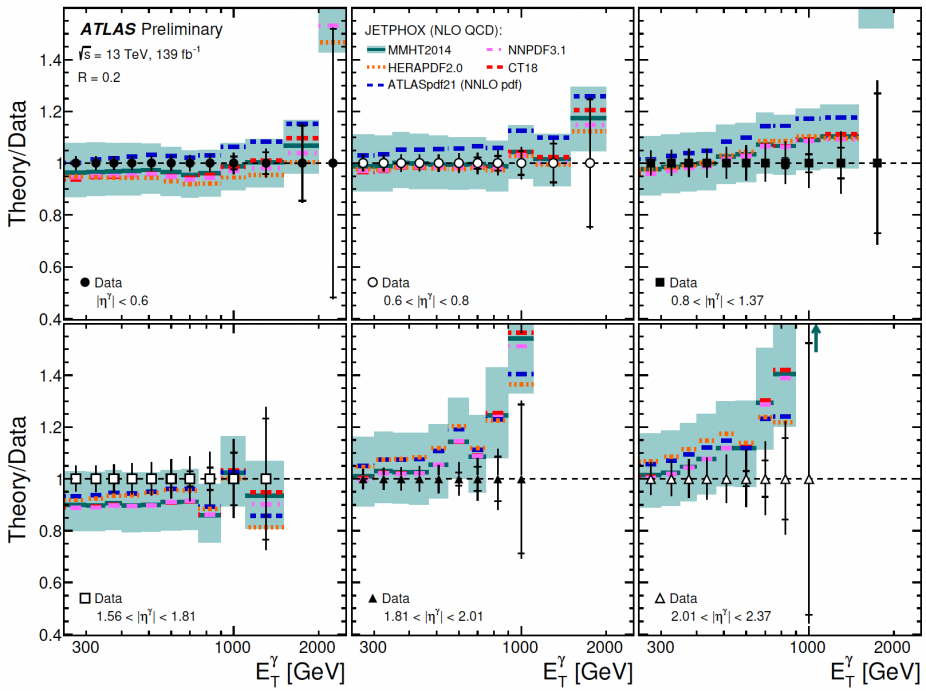

Results with $R = 0.4$

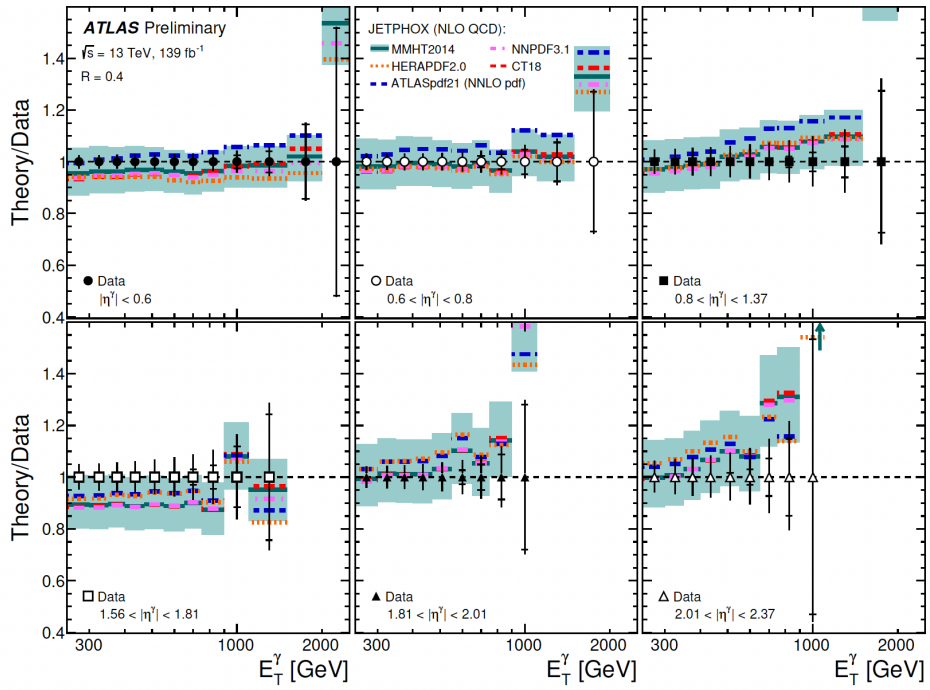

ATLAS-CONF-2022-065

→ **Adequate description of the data within experimental and theoretical uncertainties.**

Differential cross sections: data vs NNLOJET

- The measured cross sections compared to the NNLO pQCD predictions of NNLOJET as a function of E_{T}^{γ} in the different $|\eta^{\gamma}|$ regions.

→ **Scale uncertainties:** more than a factor 2 reduction with respect to NLO calculations.

Results with $R = 0.2$

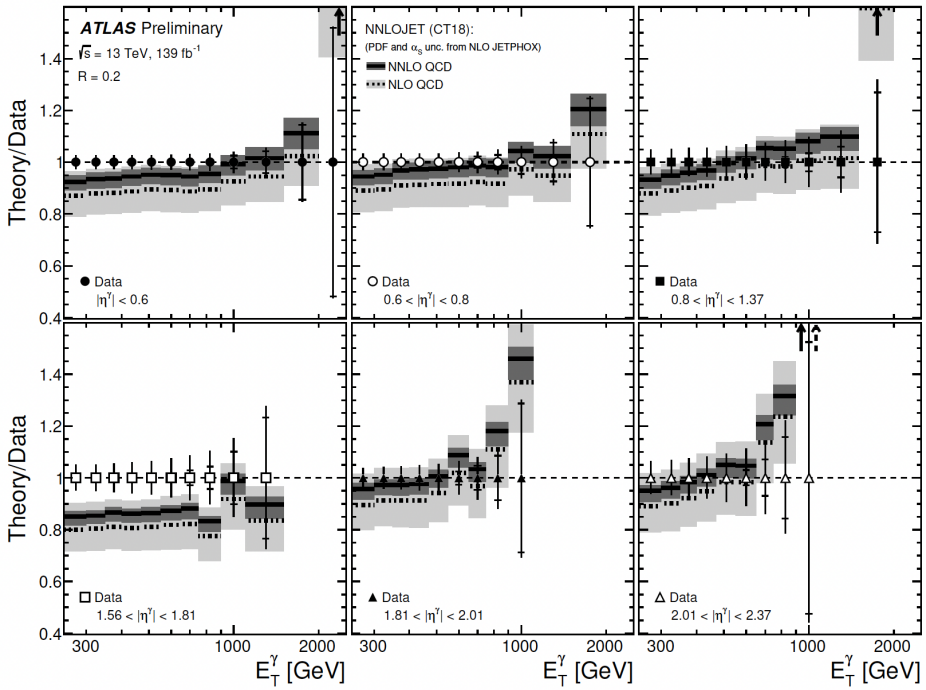

Results with $R = 0.4$

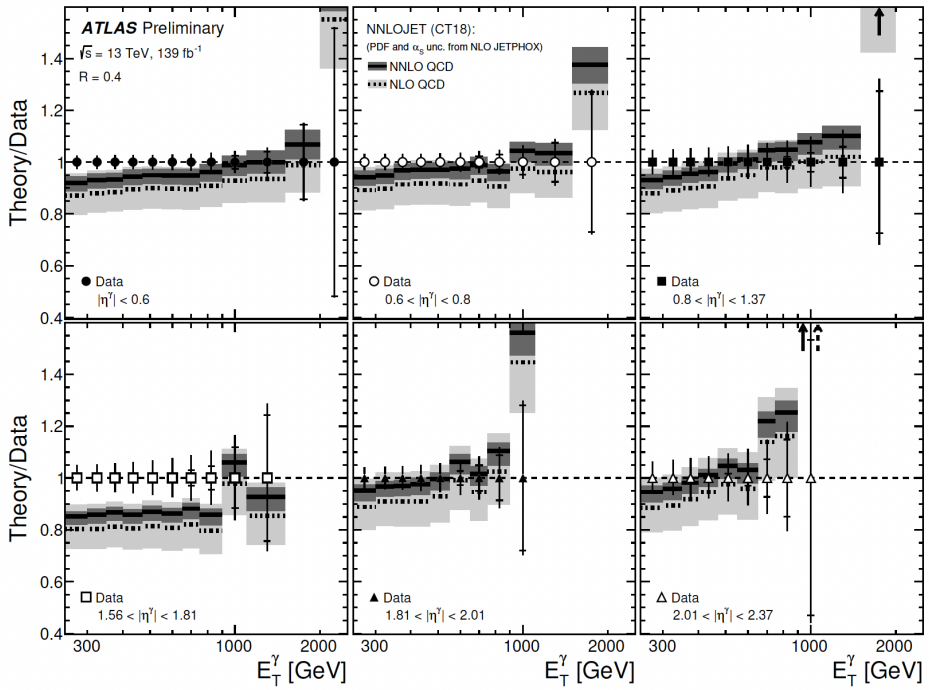

ATLAS-CONF-2022-065

→ **Predictions are consistent with the measurements within uncertainties except in the 4^{th} $|\eta^{\gamma}|$ region, where the NNLO underestimates the data.**

Fiducial cross sections: data vs SHERPA NLO

- The R-dependence of the inclusive isolated-photon cross section is tested by measuring the fiducial cross section in each $|\eta^{\gamma}|$ region for each value of R measured:

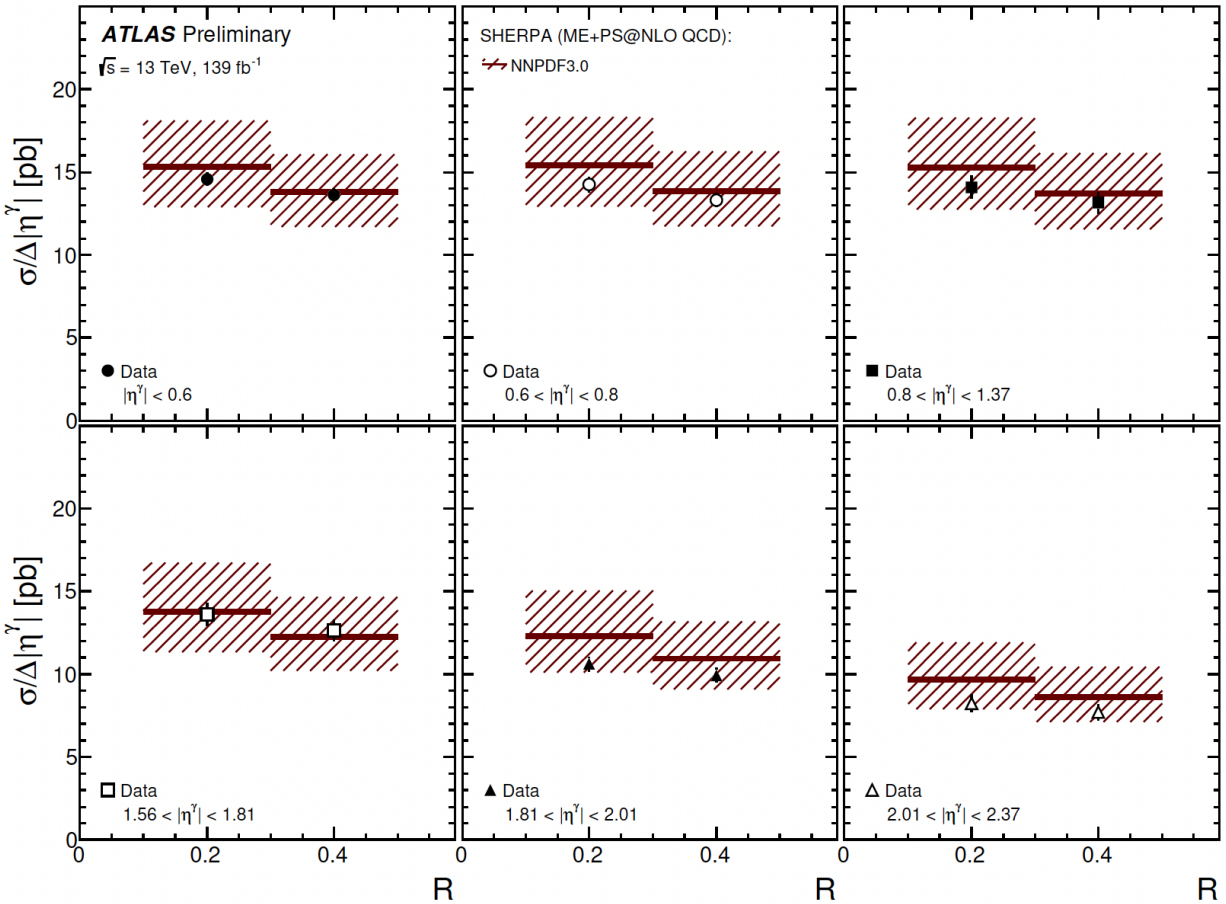

ATLAS-CONF-2022-065

→ **SHERPA NLO predictions describe the dependence of the fiducial measured cross section with R within uncertainties.**

Ratios of the differential cross sections

- Further investigation of the R dependence of the inclusive-photon cross section is performed by measuring the ratios of the cross sections for $R = 0.2$ and 0.4 as a function of E_{T}^{γ} in the different $|\eta^{\gamma}|$ regions

  $\rightarrow$ Avenue to achieve a more stringent test of the theory, with reduced experimental and theoretical uncertainties.

  $\rightarrow$ Direct test of the evolution of the R dependence with E_{T}^{γ}.

- **Treatment of uncertainty correlations**

  - **Experimental uncertainties:** all the sources were considered to be as fully correlated except for the $E_{\mathrm{T}}^{\mathrm{iso}}$ modelling.

  - **Theoretical uncertainties:** all the sources were considered to be as fully correlated.

    $\rightarrow$ **Drastic reduction of the uncertainties obtained for the ratios.**

Dominant systematic uncertainties for the ratios

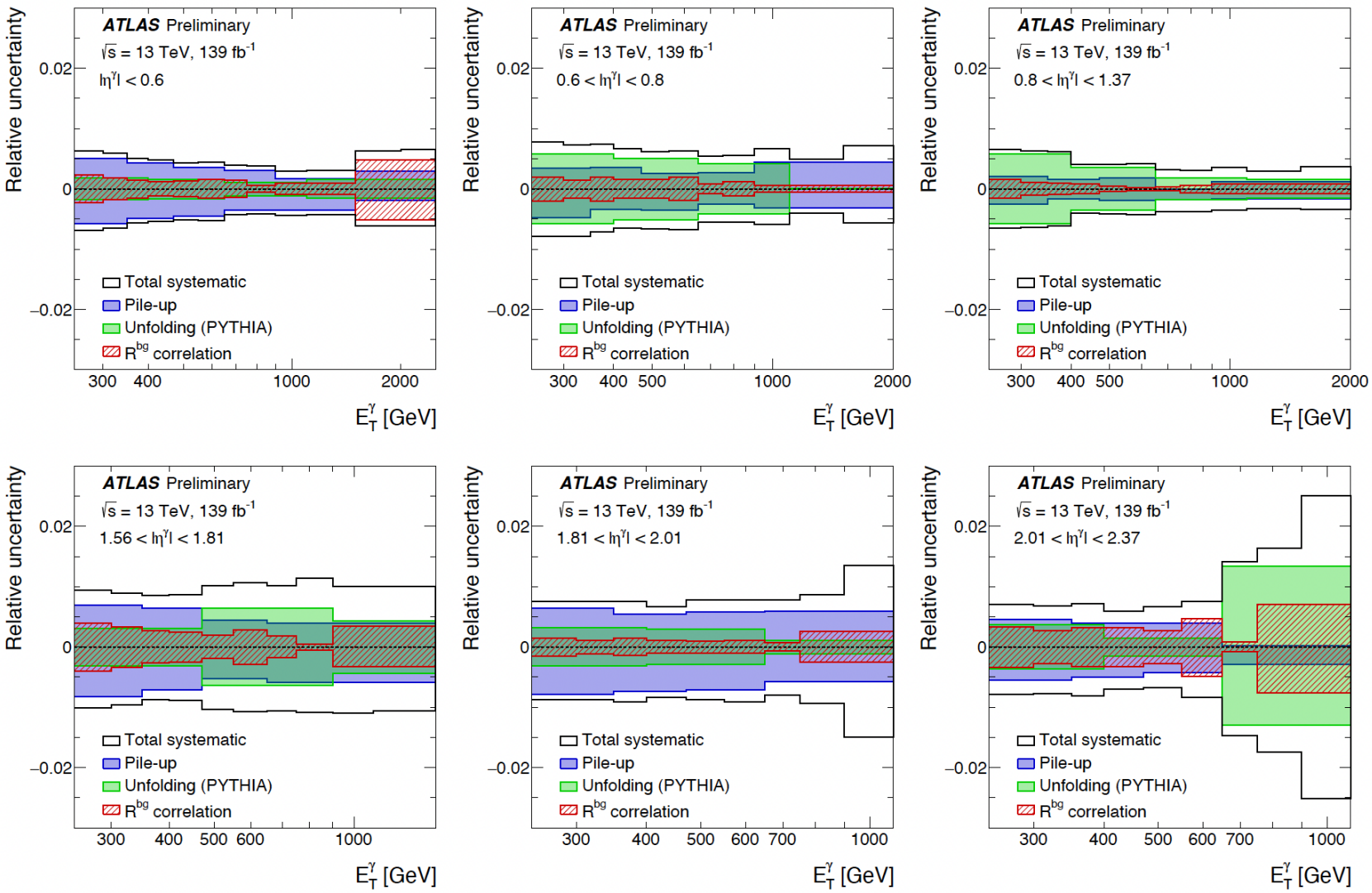

ATLAS-CONF-2022-065

→ From a $3\% - 20\%$ total uncertainty to a typically $< 1\%$ uncertainty for the ratios of differential cross sections.

Theoretical uncertainties for the ratios

- The theoretical uncertainties for the pQCD calculations of JETPHOX (left), SHERPA NLO (centre) and NNLOJET (right) are computed as fully correlated.

→ Scale variations, PDFs, α_S, and non-perturbative corrections (only for JETPHOX and NNLOJET).

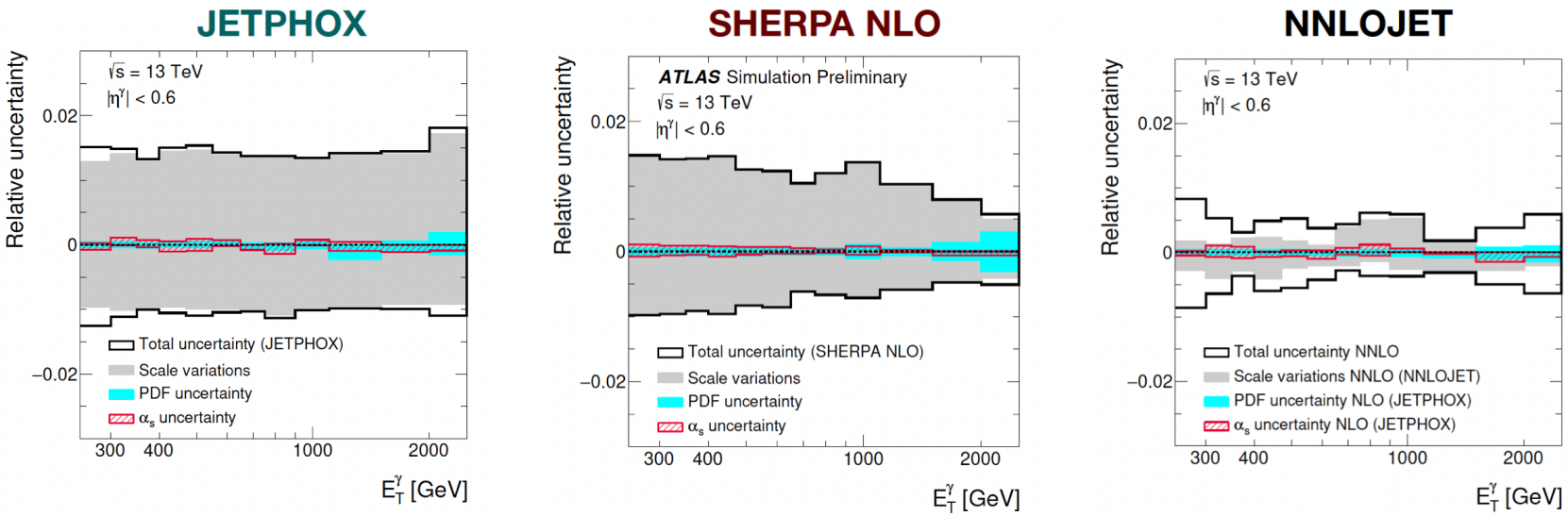

→ **Significant reduction obtained for the uncertainty on the ratios:** from a $10\% - 20\%$ $(2\% - 7.5\%)$ total uncertainty to a $\sim 1.5\%$ (1%) uncertainty for the NLO (NNLO) predictions.

ATLAS-CONF-2022-065

Ratios of the cross sections: data vs NNLOJET

- The dependence on R of the cross section is studied by measuring the ratios of the differential cross sections for $R = 0.2$ and 0.4 as a function of E_{T}^{γ} in the different $|\eta^{\gamma}|$ regions.

- **This measurement provides a very stringent test of pQCD with reduced experimental and theoretical uncertainties (order $\sim 1\%$!).**

ATLAS-CONF-2022-065

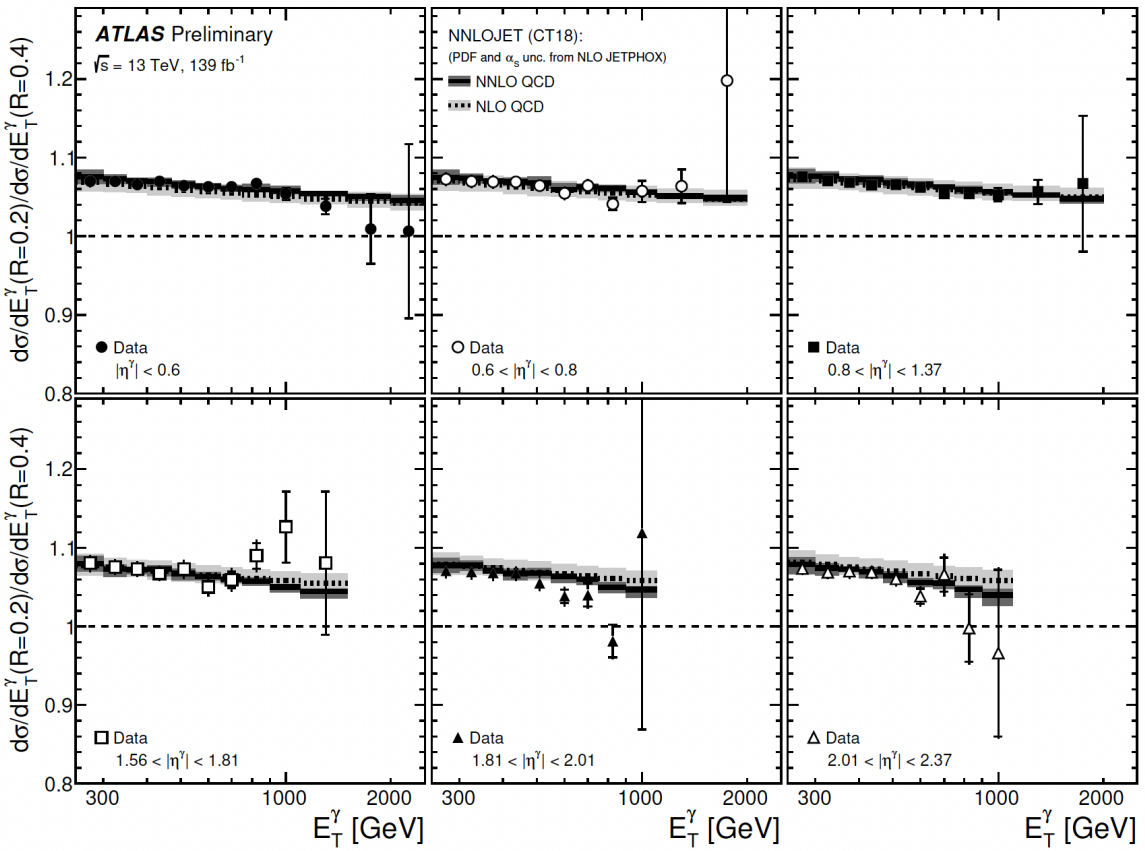

→ Validation of the underlying pQCD theoretical description up to $\mathcal{O}(\alpha_{\mathrm{S}}^2)$.

Photon plus jet at 13 TeV using the full Run-2 ATLAS data

CERN thesis: Daniel Camarero Muñoz (CERN-THESIS-2021-240)

Event and object selection

Measurement of the isolated photon+jet cross section using the full Run-2 ATLAS data.

- Differential cross sections $\mathrm{d}\sigma/\mathrm{dE}_{\mathrm{T}}^{\gamma}$ measured in three $|y^{\mathrm{jet}}|$ regions: **central** ($|y^{\mathrm{jet}}| < 1.2$), **forward** ($1.2 \leq |y^{\mathrm{jet}}| < 2.8$), and **very forward** ($2.8 \leq |y^{\mathrm{jet}}| < 4.4$).
- For each region, two configurations are measured:

Same-sign (SS): $\eta^{\gamma} \times y^{\mathrm{jet}} \geq 0$;

Opposite-sign (OS): $\eta^{\gamma} \times y^{\mathrm{jet}} < 0$.

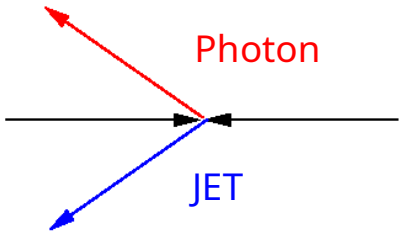

Same sign

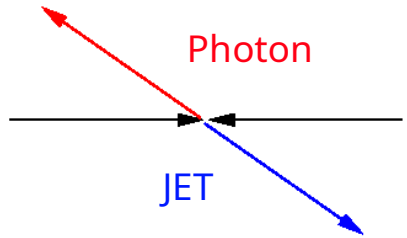

Opposite sign

- Object requirements:
  - Leading photon with $E_{\mathrm{T}}^{\gamma} > 250$ GeV and $|\eta^{\gamma}| < 2.37$ (excluding $1.37 < |\eta^{\gamma}| < 1.56$).
    - ↪ Isolation requirement: $E_{\mathrm{T,cut}}^{\mathrm{iso}}(R = 0.4) = 4.2 \times 10^{-3} \times E_{\mathrm{T}}^{\gamma} + 4.8$ GeV
  - At least one anti-k_{t} jet with $R = 0.4$, $p_{\mathrm{T}}^{\mathrm{jet}} > 165$ GeV and $|y^{\mathrm{jet}}| < 4.4$. Jets within $\Delta R^{\gamma-\mathrm{jet}} < 0.8$ were discarded.

Background subtraction and unfolding

Background subtraction:

- The ABCD method was used with signal leakage fractions from SHERPA.
- Signal purity $\gtrsim 90\%$.
  - Similar estimation obtained using either SHERPA or PYTHIA.

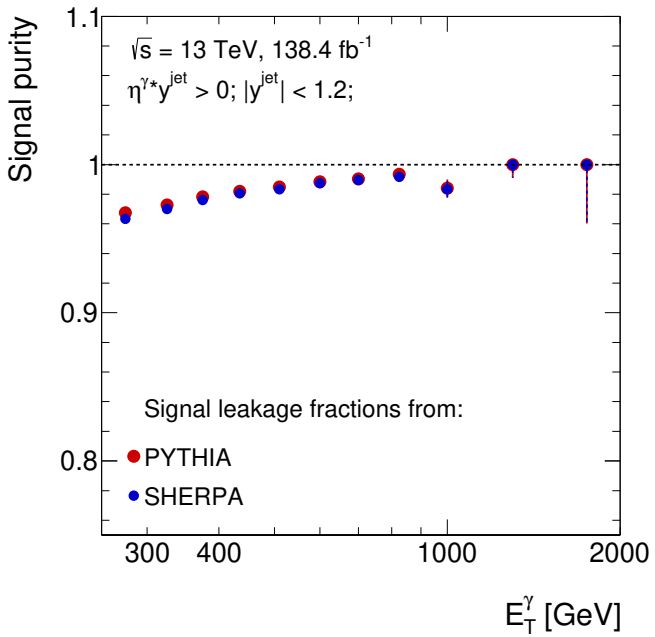

Unfolding:

- Data distributions corrected to the particle level using the Bayes method.
  - SHERPA used as nominal and PYTHIA for systematics.
  - Bin-by-bin approach used as a cross-check. Differences typically **much smaller** than 1%.

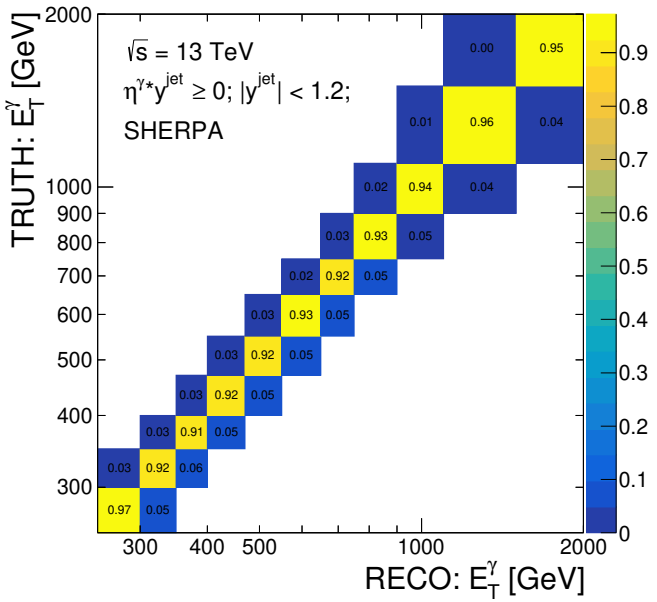

CERN-THESIS-2021-240

Jet energy scale uncertainty

In addition to the uncertainties studied for the inclusive photon analysis, the **jet energy scale** and resolution uncertainties are calculated.

- **Uncertainty evaluation:**

  The full decomposition model provided by the JetEtMiss group (113 NP) was used.

  – Each of the 113 NP was varied separately in SHERPA to estimate each systematic uncertainty.

  – A smoothing procedure was applied to each of the 113 individual components.

- **Total JES uncertainty estimation:**

  the smoothed results of the 113 individual components are added in quadrature.

  ↪ Effect on the cross section:

  Typically $< 1\%$ except for $2.8 \leq |y^{\text{jet}}| < 4.4$, where it reaches $1\% - 6\%$.

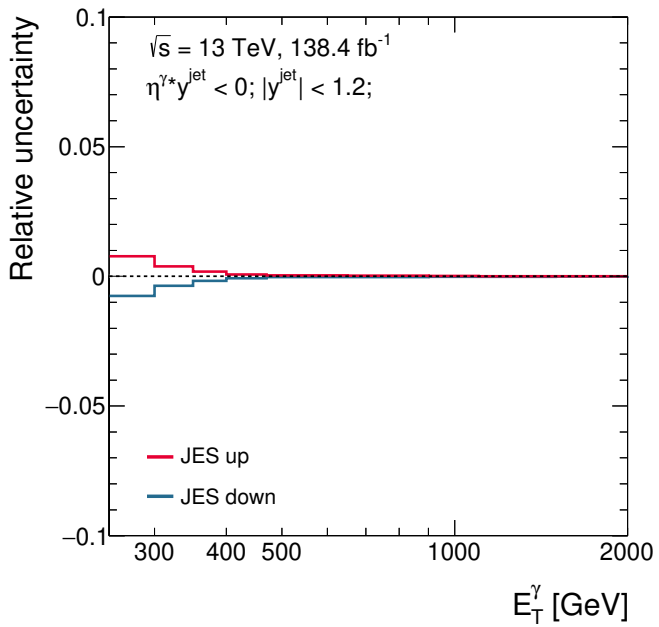

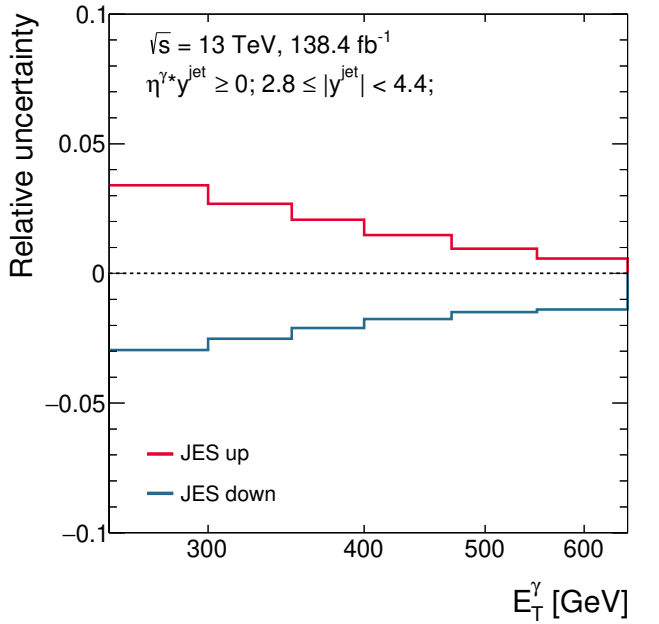

CERN-THESIS-2021-240

Systematic uncertainties

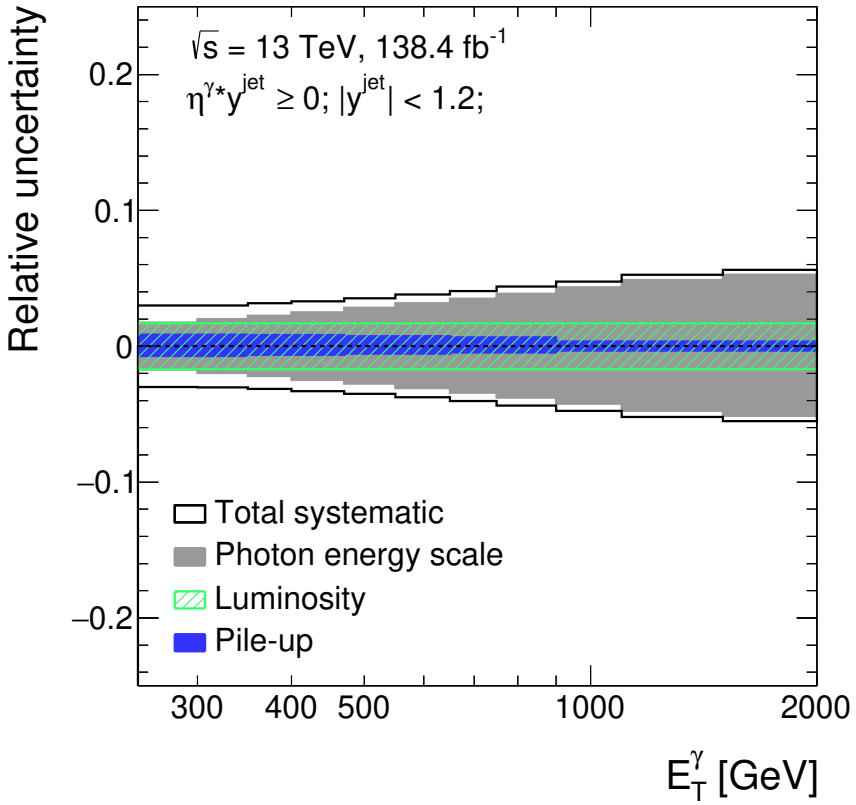

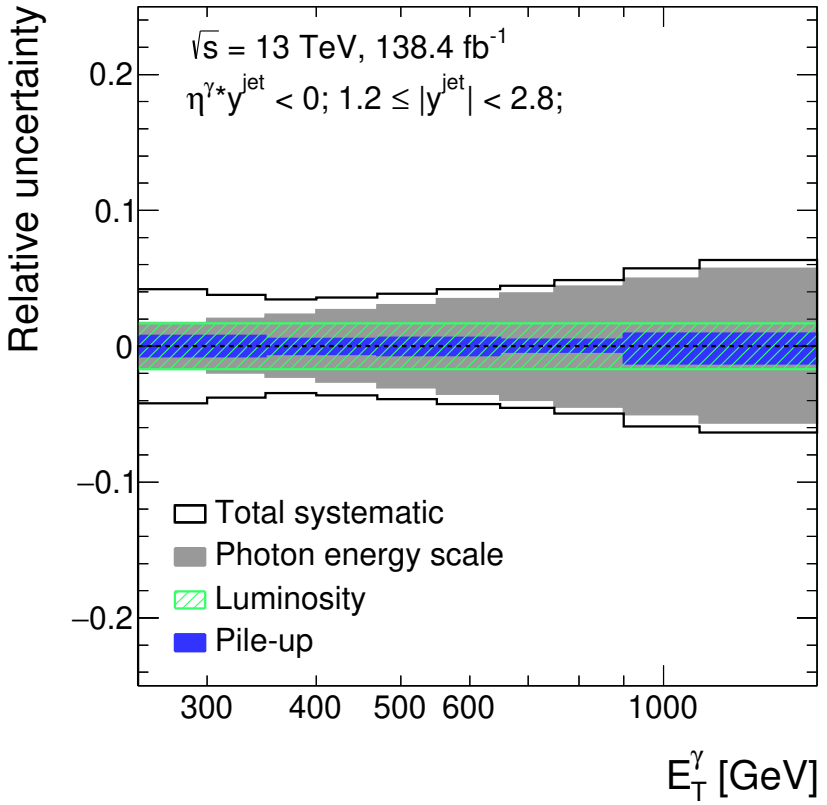

CERN-THESIS-2021-240

- The uncertainty due to the photon energy scale dominates at high-E_{T}^{γ}: values $2\% - 9\%$ $(2\% - 6.5\%)$ are reached for the SS (OS) configurations.
- The uncertainty due to the luminosity (1.7%) dominates at low E_{T}^{γ}.
- The uncertainties due to **pile-up** and $\boldsymbol{R_{\mathrm{bg}}}$ represent a significant contribution at low and medium E_{T}^{γ}: $0.5\% - 3\%$.

Differential cross sections: sensitivity to the PDFs

- Measured cross section compared with NLO pQCD predictions of SHERPA NLO for $|y^{\text{jet}}| < 1.2$ and **SS** and **OS** configurations:

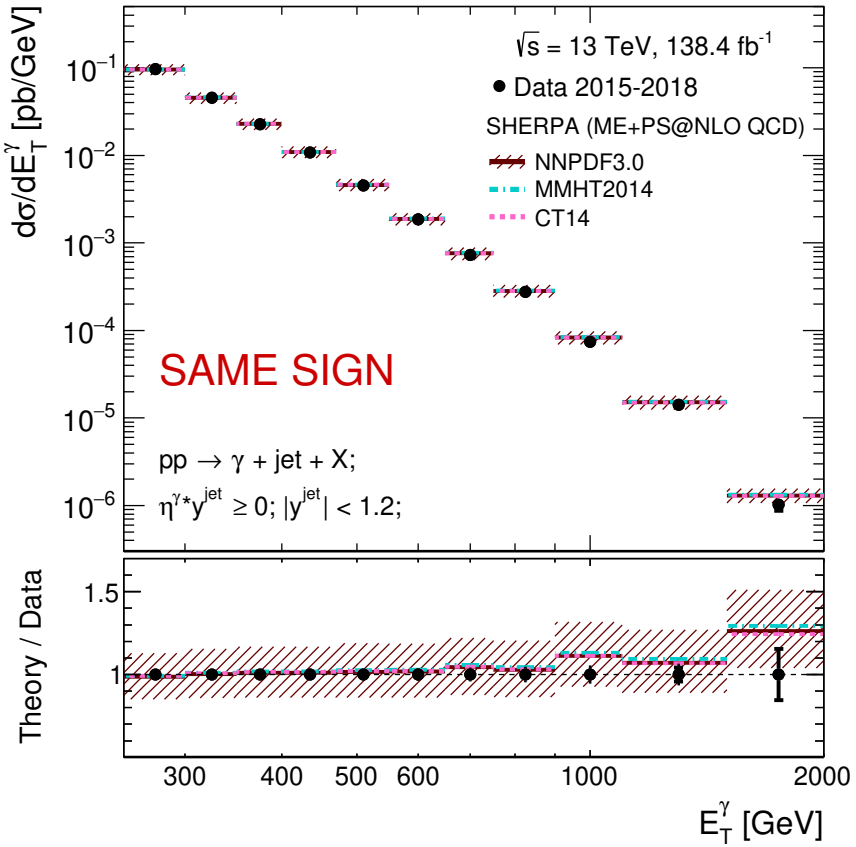

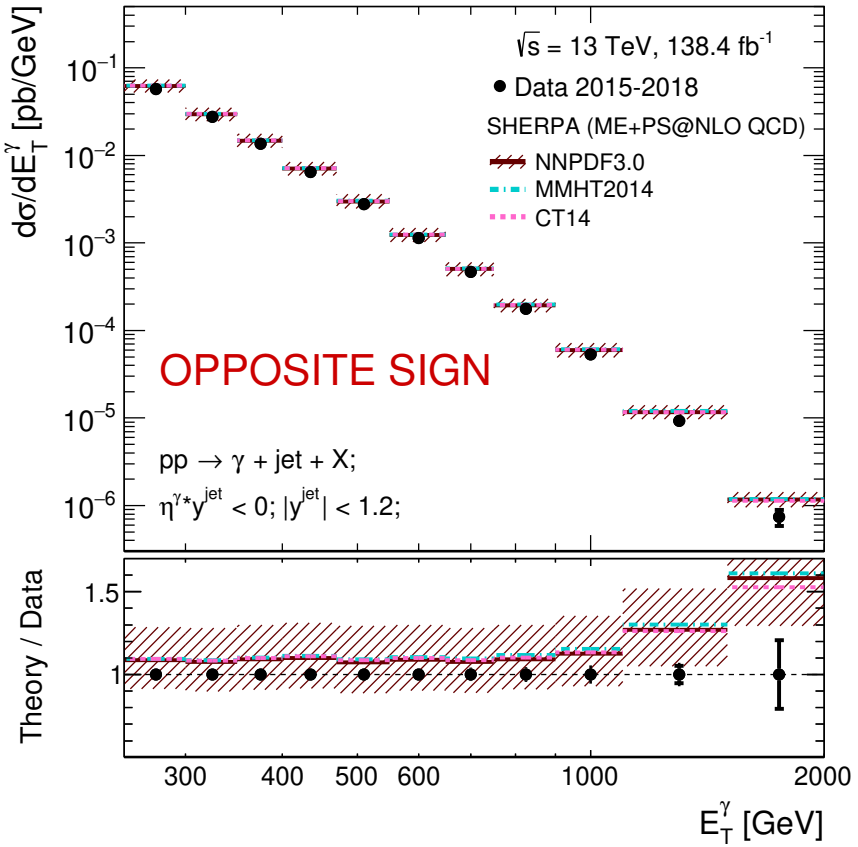

- The measurement is well described by SHERPA NLO, within uncertainties, in both **SS** and **OS** configurations.
- Mean values of x and Q^2 accessed by the measurements for the **SS** (**OS**) configurations: $\langle x \rangle = 0.080$ (0.073) and $\langle Q^2 \rangle = 1.2 \times 10^5$ GeV^2.

CERN-THESIS-2021-240

Differential cross sections: sensitivity to the PDFs

- Measured cross section compared with NLO pQCD predictions of SHERPA NLO for $1.2 \leq |y^{\text{jet}}| < 2.8$ and **SS** and **OS** configurations:

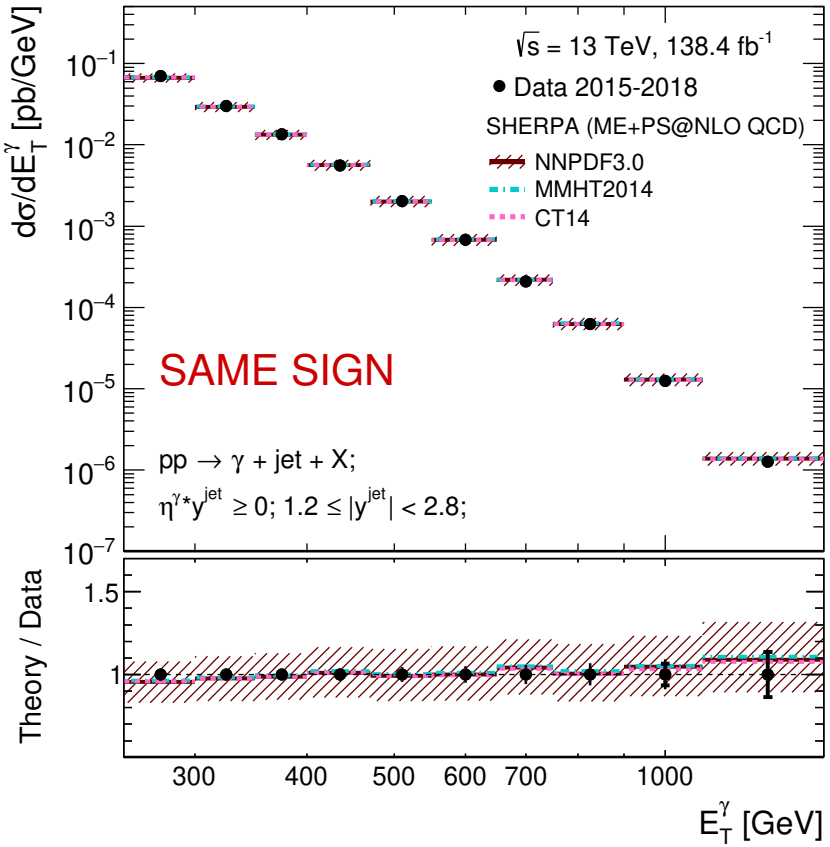

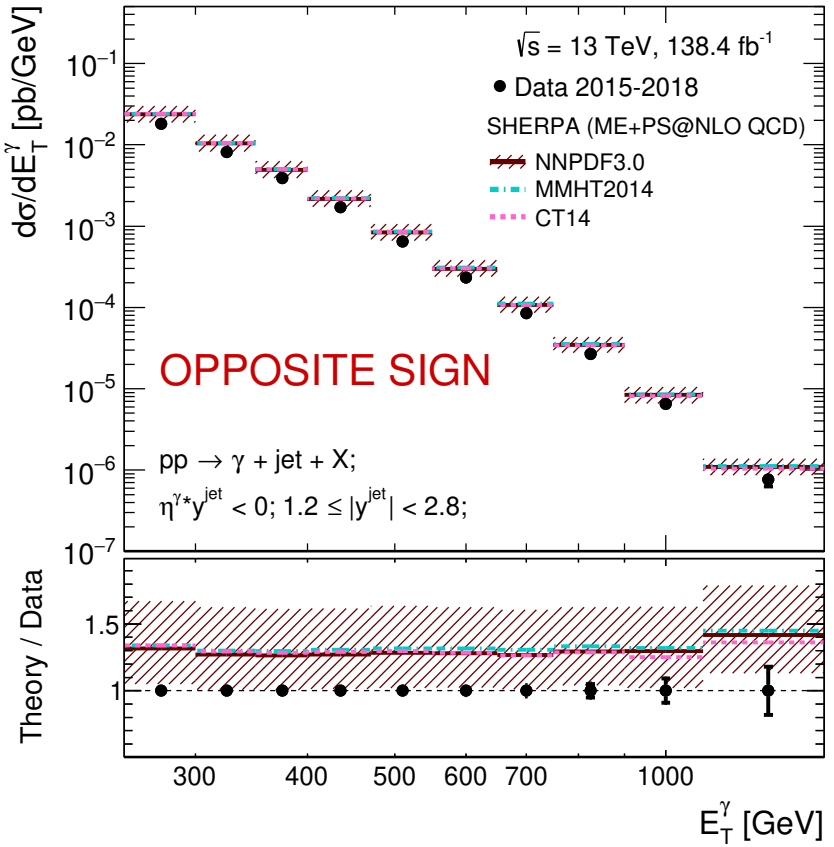

- SHERPA NLO describes well the data in the **SS**, while for the **OS** the prediction tends to overestimate the measurement.
- Mean values of x and Q^2 accessed by the measurements for the **SS** (**OS**) configurations: $\langle x \rangle = 0.133$ (0.116) and $\langle Q^2 \rangle = 1.0 \times 10^5$ (1.1×10^5) GeV^2.

CERN-THESIS-2021-240

Differential cross sections: sensitivity to the PDFs

- Measured cross section compared with NLO pQCD predictions of SHERPA NLO for $2.8 \leq |y^{\text{jet}}| < 4.4$ and **SS** and **OS** configurations:

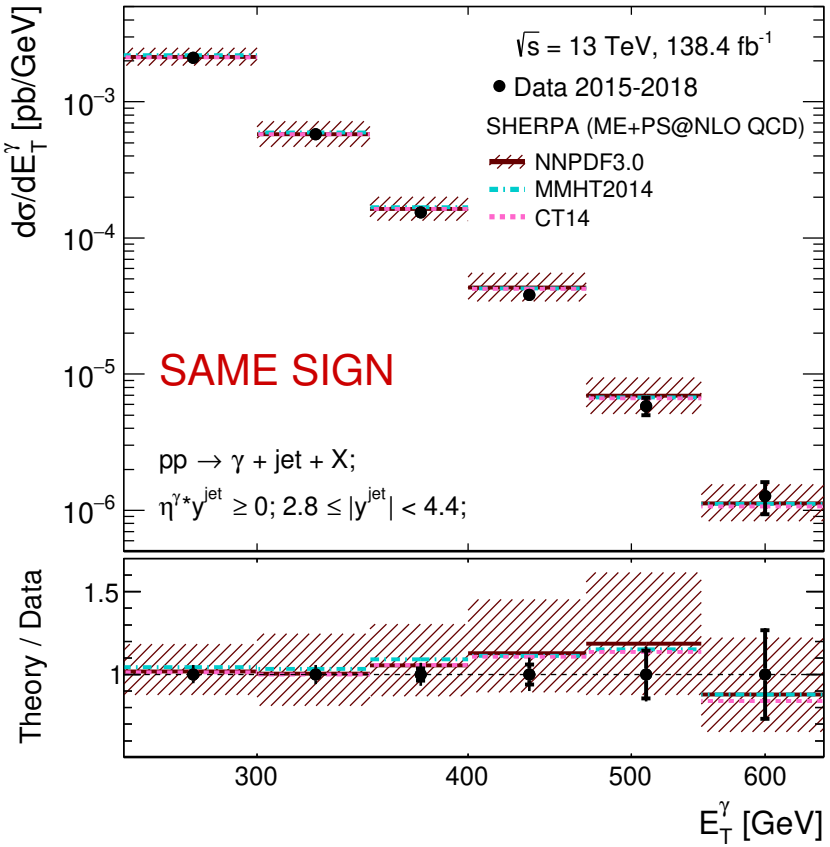

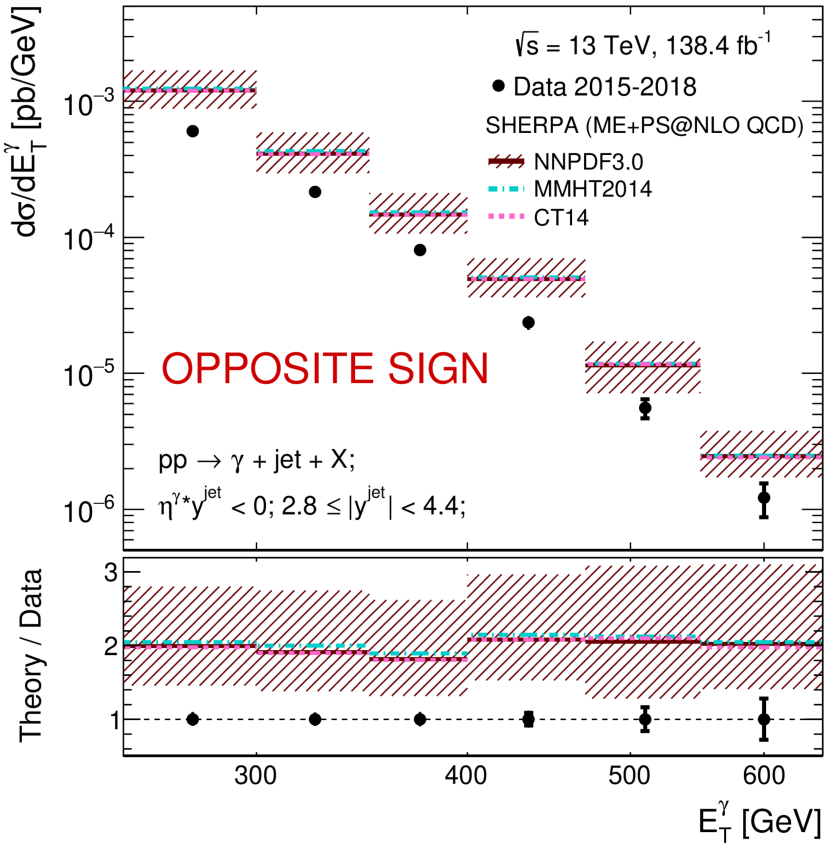

- The measurement is well described by SHERPA in the **SS**, while the prediction tends to overestimate the data in the **OS**.
- Mean values of x and Q^2 accessed by the measurements for the **SS** (**OS**) configurations: $\langle x \rangle = 0.280$ (0.275) and $\langle Q^2 \rangle = 8.5 \times 10^4$ (9.2×10^4) GeV^2.

CERN-THESIS-2021-240

Summary and conclusions

Summary and conclusions

Two cross section measurements for inclusive photon and γ+jet production in pp collisions at $\sqrt{\mathrm{s}} = 13$ TeV have been presented:

- The measurements constitute a step forward in terms of precision due to the luminosity increase and the improvements of systematic uncertainties.
- The inclusive photon cross section was measured in more $|\eta^{\gamma}|$ regions and for different γ-isolation cone R, providing more experimental information on isolation and for PDF fits.
- Photon+jet production was studied in different angular configurations to improve the sensitivity to the PDFs.
- Theoretical predictions at NLO and NNLO in pQCD were compared with the measurements, providing precise tests of the theory in the range of photon transverse energies from 250 GeV up to 2.5 TeV.
- The comparison of the ratios between data and NNLOJET predictions validates the underlying pQCD theoretical description up to $\mathcal{O}(\alpha_{\mathrm{S}}^2)$.

$\rightarrow$ Potential to constrain the proton PDFs within a global NNLO QCD fit.

Back-up

Photon identification variables

- Photon identification calorimetric variables provide good separation between prompt-photons and fake signatures from the decay of neutral hadrons in jets.

Variables used for tight identification

	LAr 1st	LAr 2nd	Hadronic
Ratios	f_1, f_{side}	R_η, R_ϕ	R_{had}
Widths	w_{s3}, w_{stot}	w_{η_2}	–
Shapes	ΔE, E_{ratio}	–	–

→ Used in the loose identification criteria

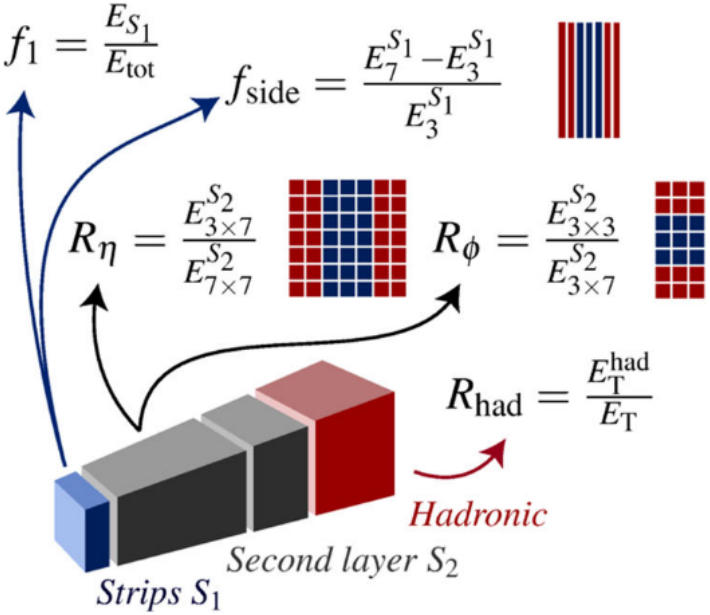

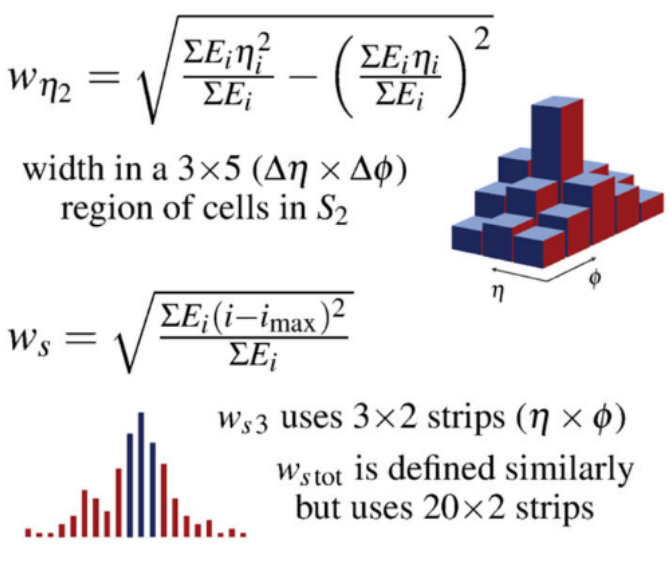

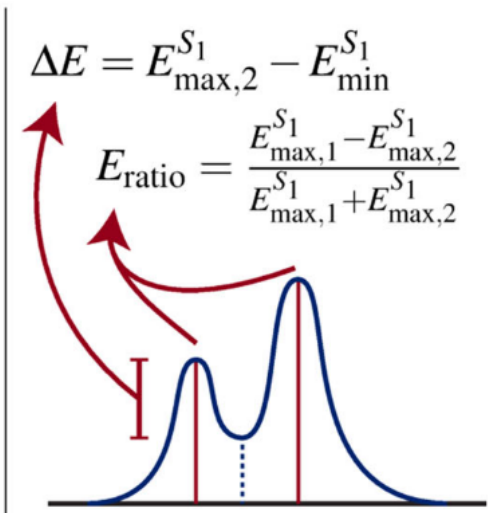

ATLAS coll., Eur. Phys. J. C **79** (2019) 205